

# My, how you've grown: a practical guide to modeling size transitions for Integral Projection Model (IPM) applications

Tom E.X. Miller<sup>\*a</sup> and Stephen P. Ellner<sup>b</sup>

<sup>a</sup>Department of BioSciences, Rice University, Houston, TX

<sup>b</sup>Department of Ecology and Evolutionary Biology, Cornell University,  
Ithaca, New York

**Running header:** Better growth modeling for IPMs

---

\*Corresponding author. Department of BioSciences, Rice University, Houston, TX 77005-1827. Email:  
tom.miller@rice.edu Phone: 713-348-4218

<sup>1</sup> **Abstract**

- <sup>2</sup> 1. Integral Projection Models (IPMs) are widely used for studying the dynamics of  
<sup>3</sup> continuously size-structure populations. IPMs require a growth sub-model that  
<sup>4</sup> describes the probability of future size conditional on current size. Over the past  
<sup>5</sup> two decades, most IPM studies have assumed that this probability is normally-  
<sup>6</sup> distributed, despite repeated calls for non-Gaussian approaches that accommodate  
<sup>7</sup> skewness and kurtosis known to occur in size transition data.
- <sup>8</sup> 2. We provide a general workflow for modeling size transitions that accommodates  
<sup>9</sup> non-Gaussian growth patterns while retaining the desirable features (ecologically  
<sup>10</sup> important covariates and random effects) that Gaussian approaches typically pro-  
<sup>11</sup> vide. Our approach emphasizes visual diagnostics of residuals from pilot Gaussian  
<sup>12</sup> models and quantile-based metrics of skewness and kurtosis that vet the fit of the  
<sup>13</sup> Gaussian distribution and guide the selection of an alternative, if necessary. We  
<sup>14</sup> illustrate our methods by reanalyzing size transition data from our published IPM  
<sup>15</sup> studies, targeting a diversity of demographic quantities including population growth  
<sup>16</sup> rate, invasion wave velocity, and evolutionarily stable life history strategies.
- <sup>17</sup> 3. Across one coral and three plant case studies, skewness and excess kurtosis were  
<sup>18</sup> common features of size transition data and non-Gaussian growth models consis-  
<sup>19</sup> tently generated simulated data that were more consistent with the real data than  
<sup>20</sup> pilot Gaussian models. However, in these case studies, the effects of “improved”  
<sup>21</sup> growth modeling on IPM results were generally modest, and differed in direction or  
<sup>22</sup> magnitude between different outputs from the same model.
- <sup>23</sup> 4. Using tools that were not available when IPMs were first developed, it is now possi-  
<sup>24</sup> ble to fit non-Gaussian models to size transition data without sacrificing ecological  
<sup>25</sup> complexity; our worked examples demonstrate how, including open-access data and  
<sup>26</sup> computing scripts. Doing so, as guided by careful interrogation of the data, will re-  
<sup>27</sup> sult in a model that better represents the population for which it is intended.

<sup>28</sup> **Keywords**

## 29 Introduction

30 Structured demographic models – matrix and integral projection models (MPMs and  
31 IPMs) – are powerful tools for data-driven modeling of population dynamics and via-  
32 bility that are widely used in basic and applied settings. In contrast to MPMs for pop-  
33 ulations with discrete structure (life stage, age class, etc.), IPMs (Easterling et al., 2000)  
34 readily accommodate populations structured by continuous state variables, most com-  
35 monly size. A related innovation of the IPM framework is its emphasis on regression-  
36 based modeling for parameter estimation, which often carries important advantages for  
37 making the most of hard-won data (Ellner et al., 2022).

38 A standard workflow allows ecologists to assemble an IPM from data using famili-  
39 iar statistical tools to describe growth, survival, reproduction, and other demographic  
40 transitions as functions of size (Coulson, 2012; Ellner et al., 2016). The relative ease of  
41 the regression-based approach, accommodating multiple covariates (e.g., environmental  
42 factors, experimental treatments) and complex variance structures (e.g., random effects,  
43 correlated errors), has facilitated a growing body of IPM literature that examines how  
44 biotic or abiotic factors affect population dynamics (e.g., Louthan et al., 2022; Ozgul  
45 et al., 2010; Schultz et al., 2017) and explores the consequences of demographic hetero-  
46 geneity associated with spatial, temporal, and individual variation (e.g., Compagnoni  
47 et al., 2016; Crone, 2016; Plard et al., 2018). The vital rate regressions (or “sub-models”)  
48 are the bridge between the individual-level data and the population-level model and its  
49 predictions; it is important to get them right.

50 Compared to other vital rates, growth is special. The regression sub-models for  
51 survival and reproduction only need to provide a single mean value as functions of  
52 size (we use “size” as the name for whatever continuous variable defines the population  
53 structure, which could instead be immune competence, mother’s weight, etc.). But for  
54 modeling growth, the full probability distribution of subsequent size, conditioned on  
55 initial size, must be defined. This distribution defines the growth ‘kernel’  $G(z', z)$  that  
56 gives the probability density of any future size  $z'$  at time  $t + 1$  conditional on current size  
57  $z$  at time  $t$ . Whenever survival and reproduction are size-dependent, the entire distribu-  
58 tion of size transitions can strongly influence IPM predictions because this distribution  
59 governs how frequently size changes are much greater or much lower than average.

60 The original template for modeling size transitions in IPMs was provided by East-  
61 erling et al. 2000. They first tried simple linear regression, assuming normally dis-  
62 tributed size changes with constant variance. Because the residuals from this regression  
63 exhibited non-constant variance, they used a two-step approach that estimated the size-

64 dependence in the residual variance (better options soon became available, such as the  
65 `lme` function in R). However, even after accounting for non-constant variance, growth  
66 data may still deviate from the assumption that size transitions are normally distributed.  
67 Size transitions are often skewed such that large decreases are more common than large  
68 increases (Peterson et al., 2019; Salguero-Gómez and Casper, 2010), or vice versa (Stub-  
69 berud et al., 2019). Size transitions may also exhibit excess kurtosis ('fat tails'), where  
70 extreme growth or shrinkage is more common than predicted by the tails of the normal  
71 distribution (Hérault et al., 2011).

72 The observation that the normal distribution may poorly describe size transitions  
73 in real organisms has been made before, and several studies have emphasized that al-  
74 ternative distributions should be explored (Easterling et al., 2000; Peterson et al., 2019;  
75 Rees et al., 2014; Williams et al., 2012). Nonetheless, default use of Gaussian growth  
76 distributions (often with non-constant variance) remains the standard practice. The gen-  
77 eral state-of-the-art in the literature appears to remain where it was 20 or so years ago,  
78 using the default model without pausing to examine critically whether or not it actually  
79 provides a good description of the data. We are guilty of this, ourselves.

80 The persistence of Gaussian growth modeling is understandable. There is a long  
81 tradition of statistical modeling built on the assumption of normally distributed resid-  
82 uals with constant variance. Popular packages such as `lme4` (Bates et al., 2007), `mgcv`  
83 (Wood, 2017), and `MCMCglmm` (Hadfield et al., 2010) make it easy to fit growth models  
84 with potentially complex fixed- and random-effect structures, but the possible distribu-  
85 tions of continuous responses are limited, and default to Gaussian. Abandoning these  
86 convenient tools for the sake of more flexible growth modeling means, it may seem,  
87 sacrificing the flexibility to rigorously model diverse and potentially complex sources of  
88 variation in growth, some of which may be the motivation driving the study in the first  
89 place.

90 The question we address here is: how can ecologists escape the apparent trade-off  
91 between realistically capturing the variance, skew, and kurtosis of size transition data  
92 on the one hand, and flexibly including the multiple covariates and random effects that  
93 often have substantial impacts on demographic rates? In this article, we offer an answer.

94 Our goal here is to present and illustrate a general and practical "recipe" that moves  
95 growth modeling past the standards set over 20 years ago, using software tools available  
96 now.<sup>1</sup> Like any recipe, users may need to make substitutions or add ingredients to  
97 suit their situation. Our approach emphasizes graphical diagnostics for developing and

---

<sup>1</sup>Our statements about what is available now are based on what tools reliably deliver in our experience, not on what they promise.

98 evaluating growth models, rather than a process centered on statistical model selection.  
99 Through a set of empirical case studies we demonstrate how a simple workflow, using  
100 tools that were nonexistent or not readily available when IPMs first came into use, makes  
101 it straightforward and relatively easy to identify when the default model is a poor fit to  
102 the data, and to then choose and fit a substantially better growth model that is no harder  
103 to use in practice. We illustrate our approach by revisiting published IPM analyses that  
104 assumed Gaussian growth, including our own previous work. In each case, the Gaussian  
105 assumption does not stand up to close scrutiny. We illustrate how we could have done  
106 better, and the consequences of “doing better” for our ecological inferences. All of our  
107 analyses may be reproduced from code and data that are publicly available (see Data  
108 accessibility statement).

## 109 A workflow for growth modeling

110 The modeling workflow that we suggest runs as follows (Fig. 1):

- 111 1. *Fit a “pilot” model or models assuming a Gaussian distribution, but allowing for non-*  
112 *constant variance.*

113 This step is familiar to most IPM users, as it is the start and end of the traditional  
114 workflow. A well-fitted Gaussian model accurately describes the mean and variance  
115 of future size conditional on current size and possibly on other measured covari-  
116 ates or random effects. This step may include model selection to identify which  
117 treatment effects or environmental drivers affect the mean and/or variance of future  
118 size. Non-constant variance is often fitted in a two-stage process, first fitting mean  
119 growth assuming constant variance, then doing a regression relating the squared  
120 residuals to initial size or the fitted mean of subsequent size. Fitting mean and  
121 variance simultaneously, as can be done with R packages **mrgcv** and **nmle**, is ad-  
122 vantageous when possible because incorrectly assuming constant variance can affect  
123 model selection for the mean. But two-step fitting may be convenient when there  
124 are multiple fixed and random effects that can affect growth variance, because the  
125 fitted mean value implicitly accounts for all of them. We illustrate both one-step and  
126 two-step approaches in the case studies below.

127 Allowing non-constant variance removes the need for transforming the data to  
128 stabilize the growth variance. Transformation remains an option when it does not  
129 create new problems (see Discussion), and it may have advantages besides variance

130 stabilization. In particular log-transformation is often appropriate for size data (Ell-  
131 ner et al., 2016), and it helps to avoid eviction at small sizes.

- 132 2. *Use statistical and graphical diagnostics to identify if and how the standardized residuals*  
133 *deviate from Gaussian, and to identify a more appropriate distribution.*

134 If the Gaussian pilot model is valid, the set of standardized residuals (standardized  
135 by the standard deviation) should be Gaussian with mean zero and unit variance,  
136 with no skew or excess kurtosis. This criterion provides a straightforward test for  
137 whether to accept a Gaussian growth model or explore alternatives. If the standard-  
138 ized residuals are satisfactorily Gaussian, skip to the final step of the workflow.

139 There are many ways that growth data may deviate from Gaussian, and the na-  
140 ture of those deviations can guide the search for a better distribution. Frequentist  
141 tests such as the D'Agostino test of skewness (D'Agostino, 1970) and the Anscombe-  
142 Glynn test of kurtosis (Anscombe and Glynn, 1983) could be used to diagnose  
143 whether the aggregate distribution of standardized residuals deviates from normal-  
144 ility (R package **moments** (Komsta and Novomestky, 2015)). However, the aggregate  
145 distribution of standardized residuals may be misleading if properties such as skew  
146 and kurtosis vary with size or other covariates. For example, a change in the di-  
147 rection of skewness from small to large sizes might produce zero overall skewness,  
148 but really requires a distribution flexible enough to accommodate both positive and  
149 negative skew, such as the skewed normal or Johnson  $S_U$  distributions. Alterna-  
150 tively, growth data may lack skew but may exhibit leptokurtosis (in which case the  $t$   
151 distribution may be a good choice) or may shift from platykurtosis to leptokurtosis  
152 depending on initial size (in which case the power exponential distribution may be  
153 a good choice). It is therefore essential to visualize trends in distribution properties  
154 with respect to size, either initial size (for simple models with only size-dependence)  
155 or expected future size (for models with multiple fixed effects). In the case studies  
156 below, we rely on quantile regression of the standardized residuals to visualize skew  
157 and kurtosis as continuous functions of initial size or expected future size. Fig. 1  
158 includes guidance on how the skew and kurtosis properties of the standardized  
159 residuals suggest options for an appropriate growth distribution. In our case stud-  
160 ies we take advantage of the many distributions provided in the **gamlss** R package  
161 (Stasinopoulos et al., 2007), but any other distributions with the necessary properties  
162 can be used.

- 163 3. *Refit the growth model using the chosen distribution.*

164 In models with multiple covariates and/or random effects, each potentially affecting

several distribution parameters (location, scale, skew, kurtosis) in different ways, “refit the model” could entail a massive model selection process to identify the “right” or “best” non-Gaussian model. And with so many options, model uncertainty may be overwhelming and over-fitting becomes a significant risk even if precautions against it are taken. We therefore argue for adopting the more modest goal of remedying any evident defects in the Gaussian model. As we demonstrate below, the functional forms for the mean and standard deviation (or location and scale parameters) can often be carried over from the pilot Gaussian model into a non-Gaussian distribution, leaving skew and kurtosis as the targets for improvement.

Our recommendation for this step is based on the fact that parameter estimation using Gaussian regression models is generally robust to deviations from normality (Schielzeth et al., 2020), meaning that the mean of the Gaussian model is probably a good proxy for the mean of the non-Gaussian model (and if it is not, the next step in the workflow would catch that). The functional forms for skew and kurtosis of the non-Gaussian model can be guided by the qualitative features of the graphical diagnostics (e.g., skewness switches from positive to negative with size).

4. *Test the final model through graphical diagnostics comparing simulated and real growth data.* A good model will generate simulated data that look like the real data. Again, it is important to inspect the properties of simulated data conditional on initial size or expected future size, rather than examining the aggregate distribution. We provide examples below of informative comparisons between simulated and real data, based mainly on quantiles. If the simulated data do not correspond well with real data, alternative (possibly more flexible) growth distributions should be explored, or more complex functions relating distribution parameters to current size and other covariates. However, we again caution against a full-blown model selection exercise. Instead, alternative models should be chosen to remedy observable discrepancies between real and simulated size transition data, and at most slightly modified based on final diagnostics and statistical tests.

## How should skewness and kurtosis be measured?

Improvement of a Gaussian model will involve scrutiny of skewness and kurtosis, so measurement of these properties warrants some attention. The standard measures of skewness and kurtosis (tail thickness) are based on the third and fourth central moments,



**Figure 1:** General workflow of recommendations for IPM growth modeling (left) and guide to common non-Gaussian distributions of size  $x$  for  $x \in \mathbb{R}$  that can accommodate different combinations of skewness and kurtosis (right). All of these distributions (often including multiple versions or parameterizations of each) are available in the package `gamlss.dist`, except for the skewed generalized  $t$ , which is available in the package `sgt` (Davis, 2015).

197 respectively, of the distribution:

$$198 \quad \text{Skewness} = \frac{m_3}{\sigma^3}, \quad \text{Excess kurtosis} = \frac{m_4}{\sigma^4} - 3 \quad (1)$$

199 where  $m_k = \mathbb{E}(X - \bar{X})^k$  is the  $k^{th}$  central moment of a random quantity  $X$  and  $\sigma^2$  is the  
200 variance (second central moment). A Gaussian distribution has zero skewness and zero  
201 excess kurtosis.

202 The standard measures are easy to calculate but their use for choosing and eval-  
203 uating growth models is hindered by their poor sampling properties. Because empirical  
204 estimates involve high powers of data values, a few outliers can produce very inaccurate  
205 estimates. Figure 2 shows a simulated example, where the underlying “data” are a sam-

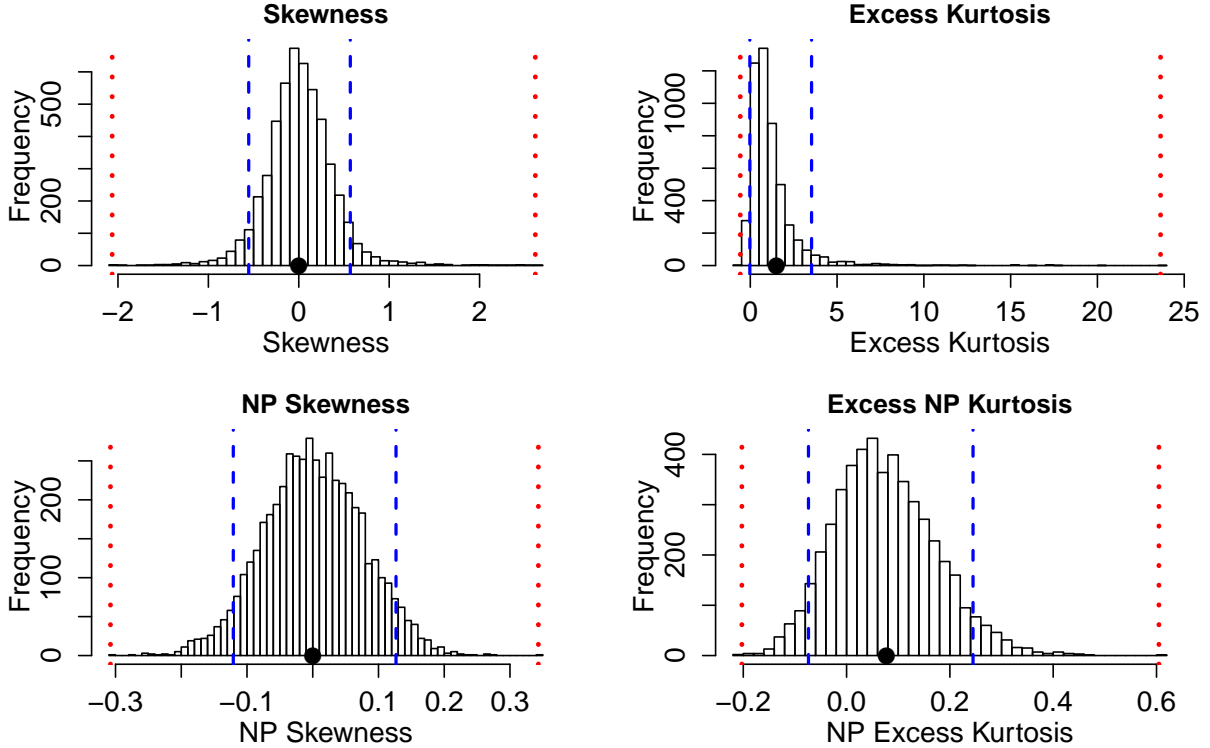


**Figure 2:** Histograms of skewness and kurtosis estimates using moment-based definitions (top two panels), compared with the nonparametric measures based on quantiles (bottom two panels). Note the very large differences in scale. Histograms are based on 5000 replicate draws of a sample of 200 independent values, from a  $t$  distribution with 8 degrees of freedom. Dotted red vertical lines mark the minimum and maximum of sample estimates, and dashed blue lines show the 5th and 95th percentiles. The true value is indicated by a black dot on the  $x$ -axis. Figure drawn by script `NPmoments.R`

ple of size 200 from a  $t$  distribution with 8 degrees of freedom; the true skew is 0, and the true excess kurtosis is 1.5. The distance between the largest and smallest estimates (indicated by the dotted red vertical lines), relative to the distance between the 5th and 95th percentiles, shows the broad extent of extreme values that can occur even with a large sample, especially for kurtosis.

We therefore use nonparametric (NP) measures of skew and kurtosis that are based on quantiles and thus are less sensitive to a few extreme values. Let  $q_\alpha$  denote the  $\alpha$  quantile of a distribution or sample (e.g.,  $q_{0.05}$  is the 5th percentile). For any  $0 < \alpha < 0.5$ , a quantile-based measure of skewness is given by (McGillivray, 1986)

$$\text{NP Skewness} = \frac{q_\alpha + q_{1-\alpha} - 2q_{0.5}}{q_{1-\alpha} - q_\alpha}. \quad (2)$$

216 NP Skewness measures the asymmetry between the tails of the distribution above and  
 217 below the median. The size of the upper tail can be measured (for any  $0 < \alpha < 0.5$ ) by  
 218  $\tau_U = q_{1-\alpha} - q_{0.5}$ ; for  $\alpha = 0.05$  this is the difference between the 95th percentile and the  
 219 median. The lower tail size is  $\tau_L = q_{0.5} - q_\alpha$ . The definition above is equivalent to

$$220 \quad \text{NP Skewness} = \frac{\tau_U - \tau_L}{(\tau_U + \tau_L)}. \quad (3)$$

221 An NP Skewness of  $\pm 0.2$  says that the difference in tail sizes is 20% of their total. The  
 222 range of possible values is -1 to 1. Both  $\alpha = 0.25$  (sometimes called “Kelly’s skewness”) and  
 223  $\alpha = 0.1$  (“Bowley’s skewness”) are common choices. We used  $\alpha = 0.1$ , unless  
 224 otherwise stated.

225 An analogous quantile-based measure of kurtosis (Jones et al., 2011) is

$$226 \quad \text{NP Kurtosis} = \frac{q_{1-\alpha} - q_\alpha}{q_{0.75} - q_{0.25}}. \quad (4)$$

227 For  $\alpha = 0.05$ , NP Kurtosis is the difference between the 95th and 5th percentiles, relative  
 228 to the interquartile range. To facilitate interpretation, we scale NP Kurtosis relative to  
 229 its value for Gaussian distribution, and subtract 1 so that the value for a Gaussian is  
 230 zero. We call this “NP Excess Kurtosis”. The value for a Gaussian distribution is zero. A  
 231 value of  $\pm 0.2$  means that the tails are on average 20% heavier (or lighter) than those of  
 232 a Gaussian with the same interquartile range. We calculate NP Kurtosis using  $\alpha = 0.05$   
 233 unless otherwise stated, to focus on the tail edges, but again this is somewhat arbitrary.

234 Figure 2C,D illustrate how, applied to exactly the same simulated samples, the non-  
 235 parametric measures produce a smaller fraction of highly inaccurate estimates caused  
 236 by a few extreme values in the sample. But also note that, in contrast to the moment-  
 237 based measures, numerically small values of the nonparametric measures (e.g., 0.1 or 0.2)  
 238 should not be disregarded, because they are both scaled so that a value of 1 indicates  
 239 extremely large departures from a Gaussian distribution.

240 Quantile-based estimation of skewness and kurtosis carries the added value that  
 241 quantile regression methods may be used to derive these properties of size transitions  
 242 as continuous functions of initial size or expected future size. In the examples below,  
 243 we sometimes use the **qgam** package to fit smooth additive quantile regression models,  
 244 which have the flexibility to accommodate nonlinear size-dependence in skewness and  
 245 kurtosis. One risk of a gam-based approach is that fitted quantiles may be too “wiggly”  
 246 without constraints on their complexity. In the examples below, we limit complexity by  
 247 fitting splines with  $k = 4$  or  $k = 6$  basis functions. For the gam-averse, other quantile  
 248 regression models may be equally suitable, and we illustrate those, too. For consistency

249 with nonparametric skewness and kurtosis, in comparisons of real and simulated data  
 250 below, we use quantile-based measures of location and scale, and use quantile regression  
 251 to visualize these as functions of size. Specifically, following Wan et al. (2014),

$$252 \quad \text{NP Mean} = \frac{q_{0.25} + q_{0.5} + q_{0.75}}{3} \quad (5)$$

253 and

$$254 \quad \text{NP SD} = \frac{q_{0.75} - q_{0.25}}{1.35}. \quad (6)$$

## 255 1 Case study: lichen, *Vulpicida pinastri*

256 We begin with a simple example where current size is the only predictor of future size.  
 257 Growth data for the epiphytic lichen *Vulpicida pinastri* were first analyzed by Shriner et  
 258 al. 2012 and analyzed again by Peterson et al. 2019 in their study of negatively skewed  
 259 growth distributions. We therefore had an *a priori* expectation of deviation from normal-  
 260 ity. The authors of the original study used a mixture distribution that separated “normal  
 261 growth or shrinkage” from “extreme shrinkage”. We aimed to fit a single, flexible growth  
 262 model that could realistically accommodate both types of size transition without requir-  
 263 ing *ad hoc* decisions about which observations of shrinkage were “extreme” or not. The  
 264 data set includes 1,542 inter-annual transitions in thallus area ( $cm^2$ ) observed from 2004  
 265 to 2009 in Kennicott Valley, AK.

266 With initial size as the only predictor, a simple way to fit a Gaussian model with  
 267 nonconstant variance is the `gam` function in `mgcv` library (Wood, 2017) using the `gaulss`  
 268 family. Following a bit of model selection, we fit the mean and standard deviation of  
 269 future size as second-order polynomials of current size, then derived the scaled residuals  
 270 from the fitted mean and sd:

```
271 # XH is the data frame
272 # t0 and t1 are initial and final thallus area, respectively
273 fitGAU <- gam(list(t1 ~ t0 + I(t0^2), ~ t0 + I(t0^2)), data=XH, gamma=1.4, family=gaulss)
274 XH$fitted_mean = predict(fitGAU, type="response")[,1]
275 XH$fitted_sd <- 1/predict(fitGAU, type="response")[,2]
276 XH$scaledResids=residuals(fitGAU, type="response")/XH$fitted_sd
```

277 Quantile regression on the scaled residuals generates the diagnostics shown in Fig. 3  
 278 (see script `Vulpicida_IPMS.R`). As expected based on previous analyses, visual analysis  
 279 of the standardized residuals indicated negative skew, especially at larger sizes (Fig. 3B).  
 280 We also find positive excess kurtosis for all sizes.

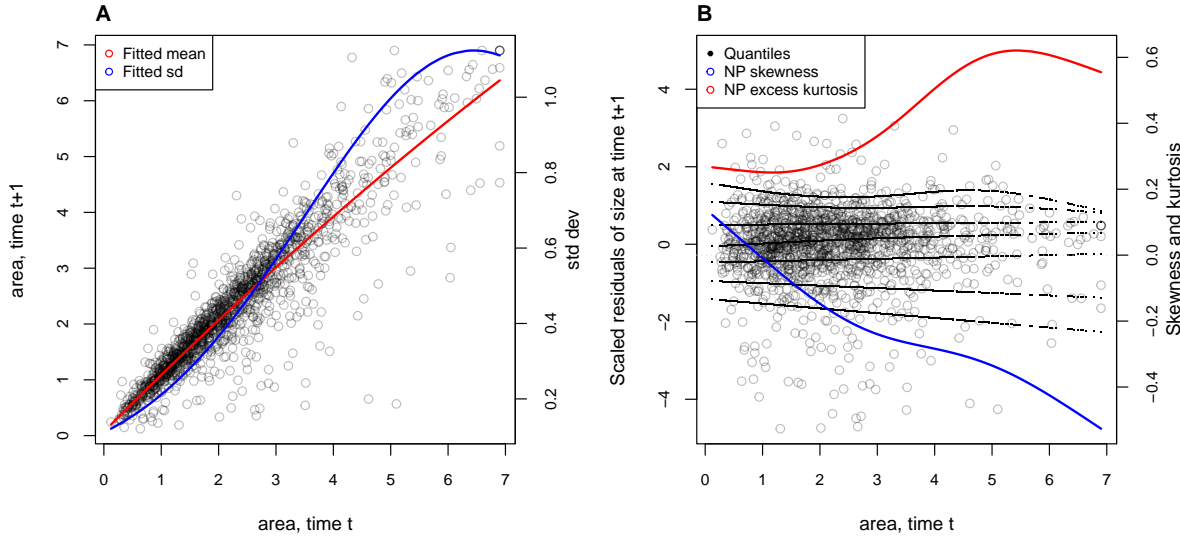


**Figure 3:** **A**, Size transition data for lichens, *Vulpicida pinastri*, and fitted gam with mean (red) and standard deviation (blue) of future size conditional on current size. **B**, Quantile regressions of scaled residuals on size and nonparametric estimates of skewness (red) and excess kurtosis (blue) derived from them. Black lines in **B** show the 5th, 10th, 25th, 50th, 75th, 90th, and 95th quantiles. Figure made by script `Vulpicida_IPMS.R`.

Lacking clear evidence of size-dependence in kurtosis, we turned to the Johnson's *S-U* (JSU) distribution for improvement. The JSU is a four-parameter, leptokurtic distribution that can accommodate positive or negative skew; it also has the convenient property that parameters `mu` and `sigma` are the mean and standard deviation, respectively, which facilitates a natural correspondence to the pilot Gaussian model. The JSU is not available as a distribution family in any of the standard linear or additive modeling packages, to our knowledge, but that need not be a barrier for this or any other distribution as long as we can write a likelihood function (`dJSU()` is provided by `gamlss`). Following the best-fit Gaussian model, we defined `mu` and `sigma` of the JSU as second-order polynomials of initial size and, based on signals of skewness and kurtosis in the standardized residuals (Fig. 3B), we define parameter `nu` (which controls skewness) as a linear function of size and `tau` (which controls kurtosis) as a positive constant; the likelihood function therefore has nine parameters to estimate. We fit the model using the `maxLik` package and starting values for `mu` and `sigma` based on estimates from the pilot Gaussian model:

```

296  ## define function that returns the JSU negative log-likelihood
297  LogLikJSU=function(pars){
298      dJSU(size_t1,

```

```

299     mu=pars[1]+pars[2]*size_t+pars[3]*size_t^2,
300     sigma=exp(pars[4]+pars[5]*size_t+pars[6]*size_t^2),
301     nu = pars[7]+pars[8]*size_t,
302     tau = exp(pars[9]), log=TRUE)
303 }
304 ## starting parameter values
305 p0<-c(coef(fitGAU22)[1:6],0,0,0)
306 ## fit with maxlik
307 outJSU=maxLik(logLik=LogLikJSU,start=p0*exp(0.2*rnorm(length(p0))),
308 method="BHHH",control=list(iterlim=5000,printLevel=2),finalHessian=FALSE);

```

309 Data simulation from the fitted JSU model indicates a compelling improvement over the  
 310 best Gaussian model, particularly in skewness and kurtosis (Fig. 4).

311 To understand the practical consequences of improved growth modeling, we as-  
 312 sembled the remainder of the lichen IPM following Shriver et al. 2012. The asymptotic  
 313 population growth rate based on Gaussian growth ( $\lambda_{GAU} = 1.001$ ) differs from the JSU  
 314 growth model ( $\lambda_{JSU} = 0.991$ ) by about 1% annual population growth, in line with re-  
 315 sults of Peterson et al. 2019. However, even this modest difference can lead to strongly  
 316 biased estimates of extinction risk from the Gaussian model, particularly over longer  
 317 time horizons (Fig. 5). We also explored differences in other life history metrics (Table).<sup>2</sup>  
 318 For example, the JSU growth model predicts values for mean lifespan, mean lifetime  
 319 reproductive success, and mean age at reproduction that are 19%, 25%, and 14% lower  
 320 than the Gaussian growth model. In this case study, properly modeling non-normal size  
 321 transitions – which was easy to do with a few extra lines of code – can have important  
 322 effects on ecological inferences.

323 One could argue that the lichen data set was a convenient “straw man” to disqualify  
 324 Gaussian growth, since it was recognized by the original and subsequent IPM analysts  
 325 that this species requires a skewed distribution of size transitions (Peterson et al., 2019;  
 326 Shriver et al., 2012). In all remaining case studies, including those in the Appendix,  
 327 we re-examine growth data that were modeled as Gaussian by the data originators in  
 328 published IPM studies.

---

<sup>2</sup>What is the best way to cite Chrissy Hernandez' life history functions?

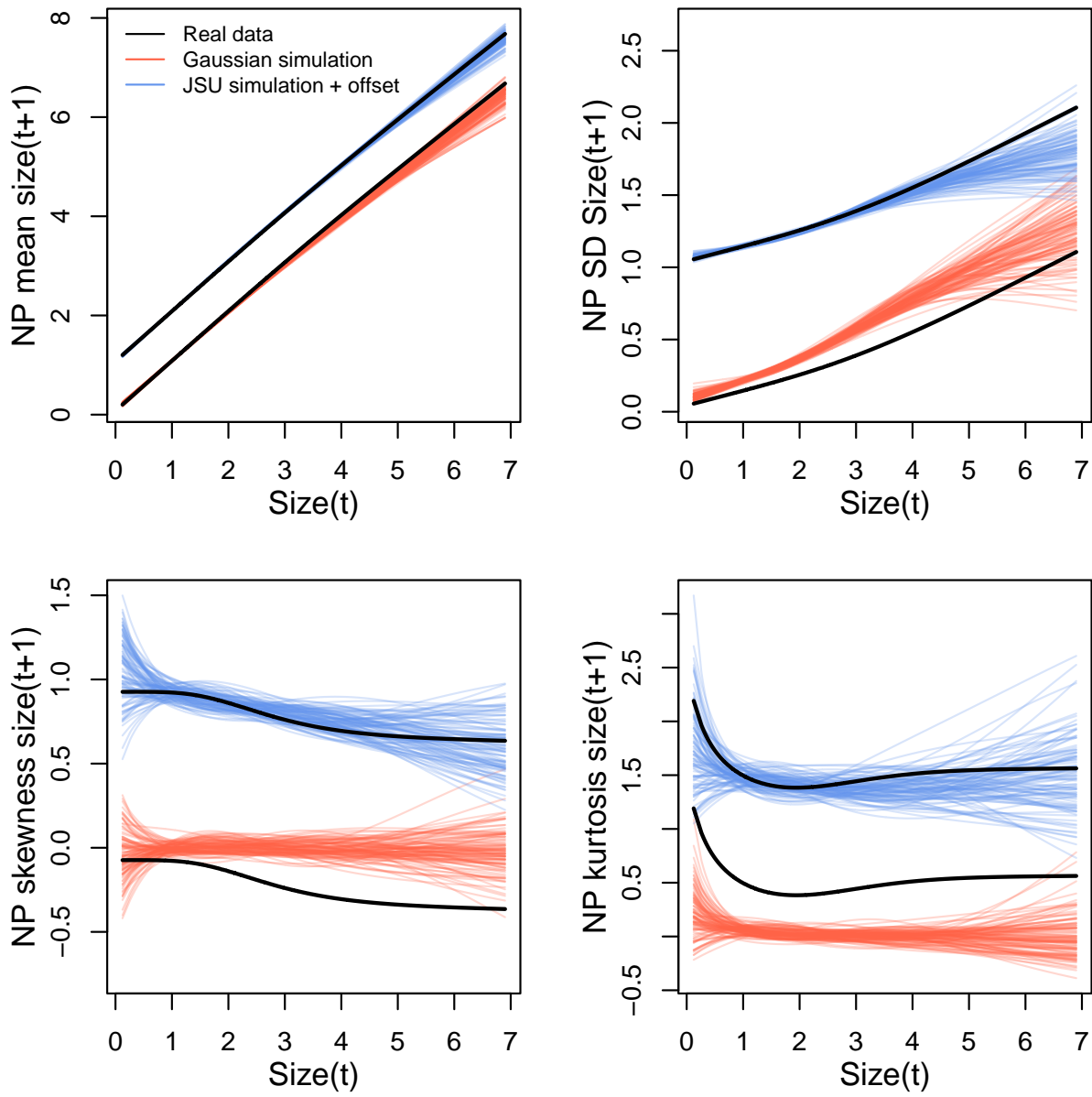


**Figure 4:** Comparisons among real lichen data and data simulated from Gaussian and JSU growth models for NP mean, NP standard deviation, NP skewness, and NP excess kurtosis of future size conditional on current size. Figure made by script `Vuplicida_IPMs.R`.

## 329 2 Case study: tree cholla cactus, *Cylindriopuntia imbricata*

330 The next case study, focusing on the tree cholla cactus *Cylindriopuntia imbricata* at the  
 331 Sevilleta Long-Term Ecological Research site in central New Mexico, adds a new feature  
 332 on top of the simple size-dependent regressions in the previous study: random effects

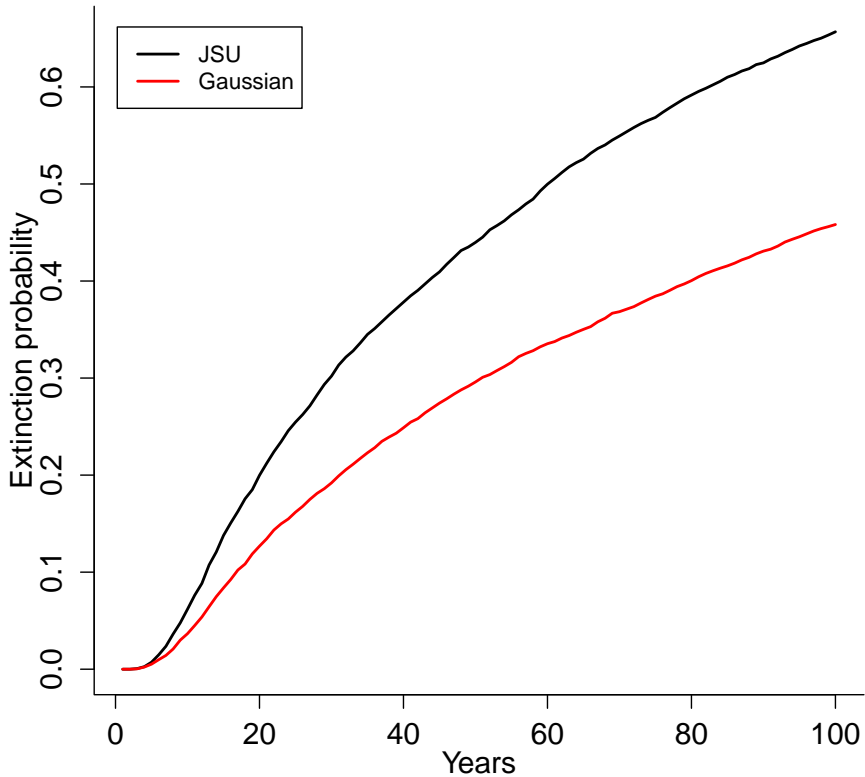


**Figure 5:** Extinction risk estimated from individual-based simulation of IPMs based on Gaussian and Johnson's S-U (JSU) growth distributions. Figure made by script Vuplicida\_IPMs.R.

associated with temporal (year) and spatial (plot) environmental heterogeneity. This long-term study of cactus demography was initiated in 2004 and different subsets of the data have been analyzed in various IPM studies, all using Gaussian growth kernels (Compagnoni et al., 2016; Czachura and Miller, 2020; Elderd and Miller, 2016; Miller et al., 2009; Ohm and Miller, 2014). In fact, (Elderd and Miller, 2016) presented a Gaussian growth model fit to the cactus data as an example of a well fit growth function, based on a marginal distribution of residuals that appeared approximately Gaussian and posterior predictive checks (PPCs) of a Bayesian model that suggested consistency between the real data and data simulated from the fitted model (Fig. 4 in (Elderd and Miller, 2016)).

While PPCs and the associated “Bayesian P-value” are popular diagnostic tools, they are often considered to be too conservative (Conn et al., 2018; Zhang, 2014), failing

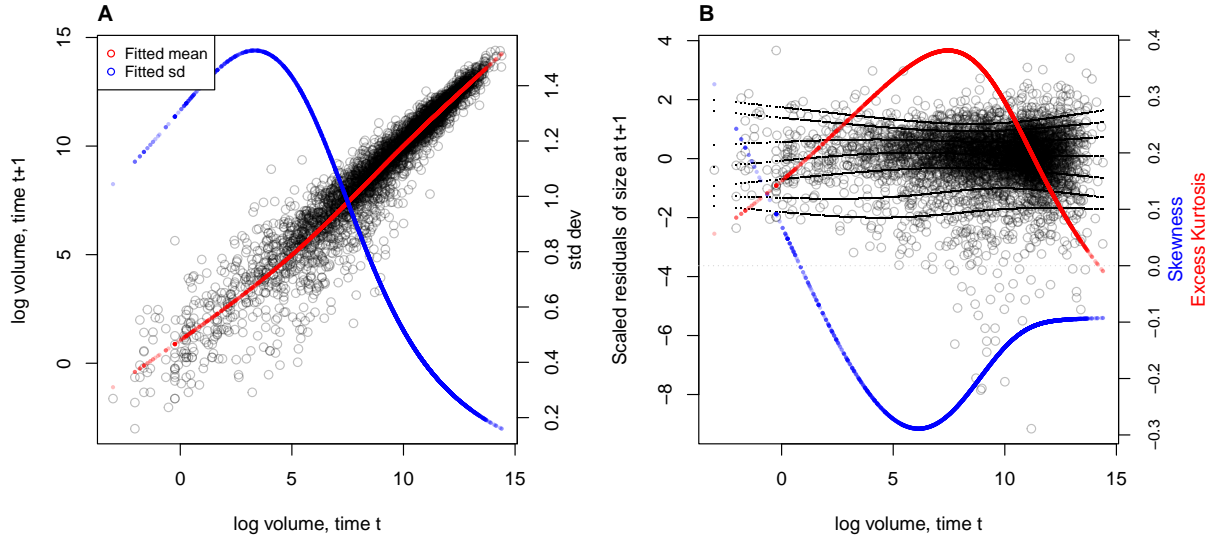


**Figure 6:** **A**, Size transition data for tree cholla cacti, *Cylindropuntia imbricata*, and fitted gam with mean (red) and standard deviation (blue) of future size conditional on current size. **B**, Quantile regressions of scaled residuals on size and nonparametric estimates of skewness (red) and excess kurtosis (blue) derived from them. Black lines in **B** show the 5th, 10th, 25th, 50th, 75th, 90th, and 95th quantiles. Figure made by script `cactus_growth_modeling_qgam.R`.

345 to reject marginally bad models even though they are very effective in rejecting models  
 346 that are terrible. The choice of discrepancy function (the statistic used to compare real  
 347 and simulated data) can also be limiting: in our previous work, we used a discrepancy  
 348 function focused on variance (the sum of the squared residuals), so we had a built-in  
 349 blind-spot for mismatches in higher moments. In the clarity of hindsight, the PPC gave  
 350 a false sense of security; the Gaussian was a poor choice all along.

351 The data for this new analysis include 4844 size transition observations from 929 in-  
 352 dividuals spanning 13 transition years (2004–2018) and 11 spatial replicates (three spatial  
 353 blocks in years 2004–2008 and eight 30m-by-30m plots in years 2009–2018). The data are  
 354 provided in Miller (2020). Following previous studies, we quantified size as the natural  
 355 logarithm of plant volume ( $cm^3$ ), derived from height and width measurements.

356 We begin the growth modeling workflow, as above, with a generalized additive  
 357 model with the mean and standard deviation of size in year  $t + 1$  modeled as function  
 358 of size in year  $t$ , with random intercepts for year and plot and assuming normally dis-  
 359 tributed residuals (`family=gaulss()`). The standardized residuals, accounting for size-  
 360 dependent residual variance (Fig. 6A), show clear signals of negative skew and positive

361 excess kurtosis across most of the size distribution but strongest in the middle of the size  
362 distribution (Fig. 6B).

363 To better capture size transitions, we need a distribution with negative skew and  
364 positive excess kurtosis, but both of which may be negligible at some sizes. We first tried  
365 Johnson's  $S_U$  and then the skewed  $t$  distributions, both of which are limited to positive  
366 excess kurtosis. Both distributions provided some improvement over the Gaussian, but  
367 were not happy with the fit of either. Iterating through the workflow (Fig. 1), we ar-  
368 rived, again, at the SHASH distribution, which is more flexible than either the JSU or  
369 skewed  $t$ , capable of capturing a greater range of kurtosis for a given amount of skew,  
370 and vice versa (Steve's NPSkewKurtosisRanges.pdf). Furthermore, fitting the SHASH  
371 as a generalized additive model with **mgcv** allowed for flexible, non-monotonic size-  
372 dependence in skewness and kurtosis without the need for model selection on specific  
373 size-dependent functions; through iterations of trial and error, we found this flexibility  
374 was necessary to generate simulated data that compared favorably to the real data. The  
375 other distributions that we tried are not available as **mgcv** families, so we fit these with  
376 custom maximum likelihood functions, an approach we illustrate in the next case study.  
377 The final growth model was similar to the SHASH gam in the coral case study, but  
378 with random intercepts for the location parameter, representing spatial and temporal  
379 heterogeneity:

```
380 fit_shash <- gam(list(logvol_t1 ~ s(logvol_t,k=4) +  
381   s(plot,bs="re") + s(year_t,bs="re"), # location  
382   ~ s(logvol_t,k=4), # log-scale  
383   ~ s(logvol_t,k=4), # skewness  
384   ~ s(logvol_t,k=4)), # log-kurtosis  
385   data = CYIM_grow,  
386   family = shash,  
387   optimizer = "efs")
```

388 The final SHASH model provided good correspondence between simulated and  
389 real data, and provided more compelling improvement over the Gaussian model than  
390 we saw in the coral case study (Fig. 7). The SHASH model over-estimated negative  
391 skew at some sizes relative to the signal of skewness in the data (Fig. 7C), but the nature  
392 of size-dependent skew in the data is not very biologically plausible and may instead  
393 be driven by the tail-wagging tendency of gams. As in the coral case study, we see  
394 that correctly modeling skewness and kurtosis improved estimation of the mean and

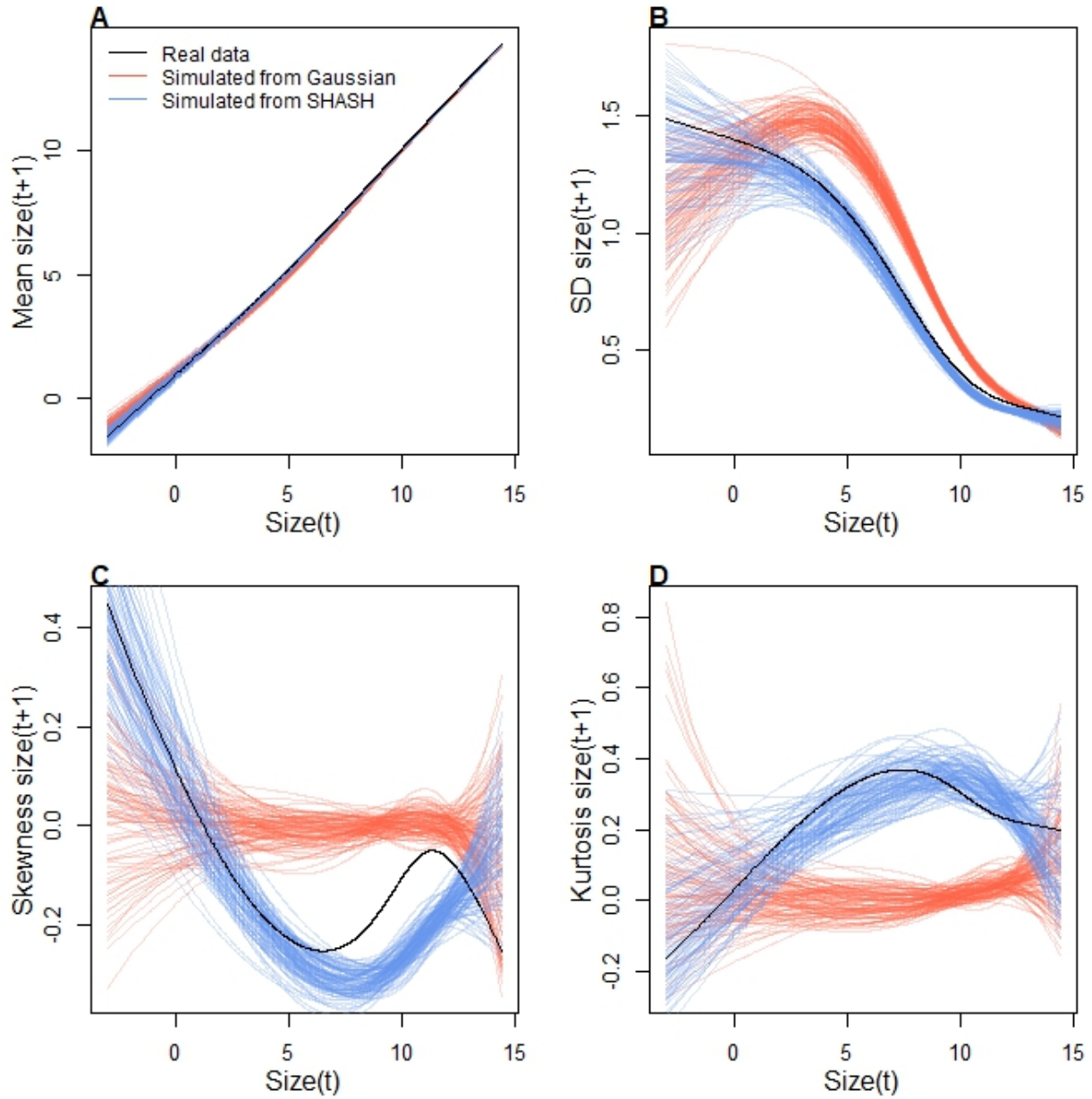


**Figure 7:** Comparisons among real cactus data and data simulated from Gaussian and SHASH growth models for mean, standard deviation, NP skewness, and NP excess kurtosis of future size conditional on current size. Figure made by script `cactus_growth_modeling_qgam.R`.

395 standard deviation (Fig. 7A,B), yielding a growth model that is clearly truer to the data  
 396 than the pilot Gaussian fit.

397 We explored how improved growth modeling influenced IPM results, leveraging  
 398 the plot and year structure of the study design to quantify spatial and temporal vari-  
 399 ance in fitness. We used the fitted random effects from the vital rate models to estimate

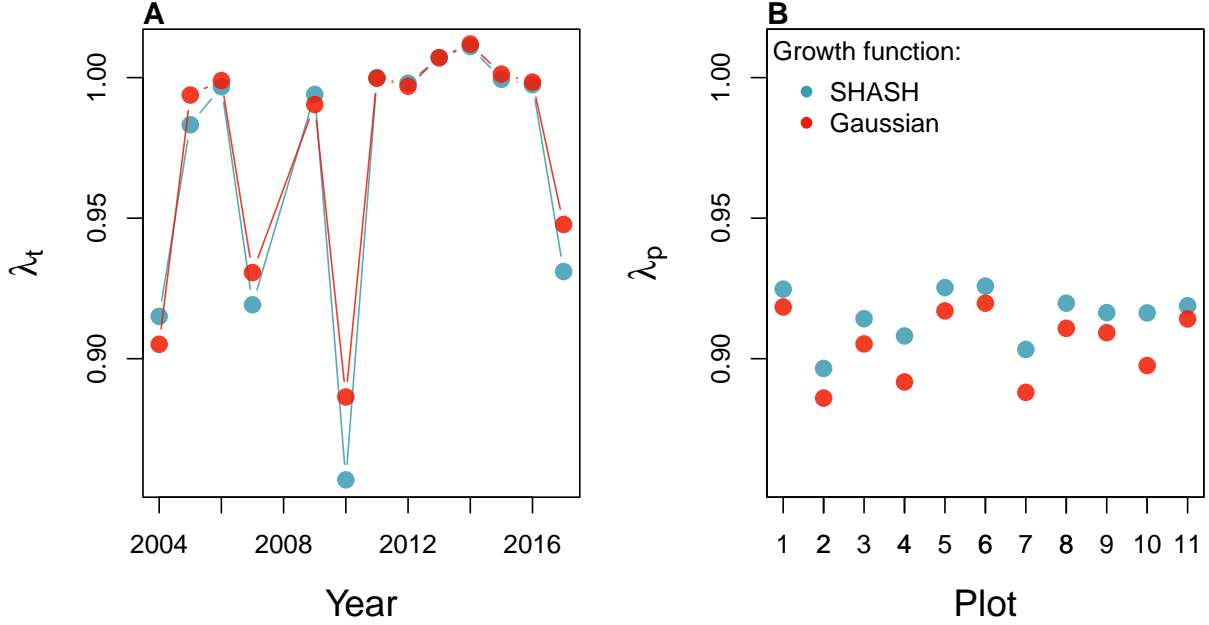


**Figure 8:** Temporal (A) and spatial (B) heterogeneity in fitness for the tree cholla cactus (*Cylindriopuntia imbricata*) predicted by IPMs using Gaussian or SHASH growth models. Figure made by script `cactus_growth_modeling_qgam.R`.

the asymptotic growth rate for each year ( $\lambda_t$ ), centered on the average plot, and for each plot ( $\lambda_p$ ), centered on the average year. This allowed us to quantify demographic variance associated with temporal and spatial heterogeneity. We found that the Gaussian growth model tended to over-estimate  $\lambda_t$ , particularly in the harshest years (Fig. 8A), and thus under-estimated temporal variance in fitness ( $Var(\lambda_{t(Gaussian)}) = 0.0018$ ,  $Var(\lambda_{t(SHASH)}) = 0.0023$ ). The opposite was true for plot-to-plot variation (Fig. 8B), where the Gaussian model under-estimated  $\lambda_p$  and over-estimated spatial variance in fitness ( $Var(\lambda_{p(Gaussian)}) = 0.00015$ ,  $Var(\lambda_{p(SHASH)}) = 0.000088$ ). Across both growth models, fluctuations in fitness were stronger through time than across space. The difference in temporal variance would suggest that Gaussian growth modeling would lead to over-estimation of the stochastic growth rate  $\lambda_S$ , since temporal variance has a negative influence on  $\lambda_S$ . However, this was not the case: stochastic IPMs based on Gaussian and SHASH growth models had nearly identical stochastic growth rates ( $\lambda_S(Gaussian) = 0.9906$ ,  $\lambda_S(SHASH) = 0.9909$ ). This is likely because temporal fluctuations in vital rates, which is where the SHASH growth model would make a difference, have a weaker influence on  $\lambda_S$  than the temporal fluctuations in size structure that they generate (Compagnoni et al., 2016; Ellis and Crone, 2013). Thus, depending on the target of one's analysis, modeling non-Gaussian size transitions with a Gaussian growth model could bias results in either direction, or make no difference at all.

### <sup>419</sup> 3 Case study: creosotebush, *Larrea tridentata*

<sup>420</sup> Our next case study comes from our studies of the woody shrub creosotebush (*Larrea tri-*  
<sup>421</sup> *dentata*) at the Sevilleta Long-Term Ecological Research (LTER) site in central New Mex-  
<sup>422</sup> ico, US. At this site as elsewhere in the Southwest US, creosotebush is encroaching into  
<sup>423</sup> desert grassland habitats. The data described here were collected along transects span-  
<sup>424</sup> ning grass-shrub ecotones to understand patterns of density dependence in creosotebush  
<sup>425</sup> demography. Specifically, we asked whether fitness is maximized approaching zero den-  
<sup>426</sup> sity at the leading edge of the expansion front (consistent with ‘pulled’ expansion), or  
<sup>427</sup> whether there is a demographic advantage for shrubs at higher density due to positive  
<sup>428</sup> feedbacks expected for ecosystem engineers (leading to ‘pushed’ expansion). Our pub-  
<sup>429</sup> lished study (Drees et al., 2023) used a spatial integral projection model (SIPM) to predict  
<sup>430</sup> the speed of shrub encroachment, assuming normally-distributed size transitions. Here  
<sup>431</sup> we step through our suggested workflow to ask whether a non-Gaussian model would  
<sup>432</sup> have been more faithful to the data, and how such an improvement would influence  
<sup>433</sup> predictions for the speed of encroachment. We use this case study to illustrate several  
<sup>434</sup> new elements and challenges, including modeling skewness and kurtosis as functions of  
<sup>435</sup> expected future size (instead of initial size) and using distributions that are not available  
<sup>436</sup> as **mgcv** families. In fact, to diversify our use of software and illustrate alternatives, we  
<sup>437</sup> do not use **gam**’s for any element of this case study.

<sup>438</sup> Growth data come from 522 shrubs censused longitudinally over four years (2013-  
<sup>439</sup> 2017). Census individuals occurred along 12 replicate transects (200 to 600 m in length)  
<sup>440</sup> that spanned gradients of shrub density along shrub-grass ecotones. Size was measured  
<sup>441</sup> as volume of an elliptical cone based on height and width measurements; the size vari-  
<sup>442</sup> able of the IPM was the natural logarithm of volume ( $cm^3$ ). For each census individual,  
<sup>443</sup> we recorded the size and density of all conspecifics within the five-meter transect “win-  
<sup>444</sup> dow” in which it occurred, and took the sum of all sizes within the window as a measure  
<sup>445</sup> of local density. The data are available in Ochocki et al. (2023).

<sup>446</sup> As an initial Gaussian approach, we first fit a set of candidate linear mixed mod-  
<sup>447</sup> els, including transect as a random effect, that represented competing hypotheses for  
<sup>448</sup> how size, density, and their interaction influence growth. Specifically, we fit five can-  
<sup>449</sup> didate Gaussian models that included fixed effects of initial size only (model 1), size  
<sup>450</sup> and density (model 2), and size, density, and their interaction (model 3), allowing for  
<sup>451</sup> shrubs of different sizes to have different growth responses to local density. Models 4  
<sup>452</sup> and 5 mirrored models 2 and 3 but included second-order terms for density, allowing  
<sup>453</sup> for the possibility of non-monotonic density dependence. As in (Drees et al., 2023) we

454 pooled data across three transition years. Initial AIC rankings of these pilot models fa-  
 455 vor model 4 slightly over model 5 ( $\Delta AIC = 0.8$ ) and significantly over all other models  
 456 ( $\Delta AIC > 2$ ). However, these models were fit assuming constant variance, and inspection  
 457 of the residuals of the best model indicate this is not a safe assumption.

458 Unlike our previous case studies, here we have multiple fixed effects that may influ-  
 459 ence the variance of future size. In cases such as this, we recommend modeling variance  
 460 as a function of expected future size, rather than initial size as we did with the corals  
 461 and cacti. The expected (or “fitted”) values reflect the combined influence of all fixed  
 462 and random effects, and therefore implicitly account for multiple sources of variation in  
 463 the variance. While there are several convenient software packages for simultaneously  
 464 modeling Gaussian mean and variance as functions of independent variables (**mgcv** for  
 465 gam models as we saw above, **nlme** for linear models), **modeling variance as a function**  
 466 **of the mean is trickier because they cannot easily be fit simultaneously**<sup>3</sup>. Here we us an  
 467 iterative re-weighting approach – which is not elegant, but it works. For Gaussian mod-  
 468 els, weights  $w_i$  can be used to indicate that the observations  $y_i$  vary in their dispersion  
 469 around the mean. In general, the iterative steps are:

1. Fit the expected value and normally-distributed residuals with constant variance:

$$y_i = \mu_i + \epsilon_i$$

$$\epsilon_i \sim N(0, \sigma)$$

2. Fit the standard deviation of the residuals as a function of the expected value.

Weights are derived as the inverse of the fitted variance:

$$\epsilon_i \sim N(0, f(\mu_i))$$

$$w_i = 1/f(\mu_i)^2$$

3. Re-fit the observation model, weighting the residual variance according to step 2:

$$y_i = \mu_i + \epsilon_i$$

$$\epsilon_i \sim N(0, \sigma \times \sqrt{w_i})$$

470 We iterated steps 2 and 3 until the weights did not change. In step 2, we modeled  
 471 the standard deviation as a simple linear function of the expected value ( $\log(f(\mu_i)) =$   
 472  $\beta_0 + \beta_1 * \mu_i$ ) but other functions are possible, as is model selection among them. We

---

<sup>3</sup>After I wrote this I discovered that **nlme** can fit residual variance as a function of fitted(.).

473 did this for all candidate models and, for fair AIC comparison, we re-fit all candidate  
 474 models with the same weights, estimated from the top model. The updated model  
 475 selection continued to favor model 4, but now with a stronger improvement over the  
 476 next-best model ( $\Delta AIC = 3.0$ ).

477 The resulting Gaussian growth model predicts strong initial size-dependence and  
 478 weak and slightly nonlinear (but monotonic) negative density dependence (Fig. 9A).  
 479 The model accounts for non-constant variance through the fitted weights, which in-  
 480 dicate greater dispersion for smaller values of expected size ( $\beta_1 = -0.21$ ; Fig. 9B).  
 481 mostly Quantiles of the standardized residuals indicate size-dependent mostly negative  
 482 skew and positive excess kurtosis, especially at smaller expected sizes (Fig. 9C).<sup>4</sup> As a  
 483 candidate for improvement, we turned to the Johnson's  $S_U$  (JSU) distribution, a four-  
 484 parameter, leptokurtic distribution capable of skew in either direction.

485 Following our suggested workflow, rather than re-fitting a JSU model from scratch,  
 486 we parameterize a model a model where the residuals from the Gaussian "pilot" model  
 487 are fitted by a JSU distribution. This relatively easy because the **gamlss.dist** package  
 488 provides a parameterization of the JSU in which the location parameter  $\mu$  is the mean  
 489 and scale parameter  $\sigma$  is the standard deviation (Rigby et al., 2019). Using that, we  
 490 fit the "hybrid" model by writing a likelihood function that uses the fitted mean and  
 491 standard deviation functions from Gaussian pilot model, and estimates the parameters  
 492 that control skewness and kurtosis as linear functions of predicted future size. The  
 493 "hybrid" likelihood looks like this SPE: if we are going to use the spline SD function,  
 494 this will need to change:

```
495 ## log_volume_t1 are the size obervations
496 ## GAU_fitted are the predicted future size from the best Gaussian model
497 ## pars is a vector of free parameters to be estimated
498 JSULogLik=function(pars){
499   dJSU(x=log_volume_t1,
500         mu=GAU_fitted,
501         sigma=exp(GAU_sd_coef[1]+GAU_sd_coef[2]*GAU_fitted),
502         nu = pars[1]+pars[2]*GAU_fitted,
503         tau = exp(pars[3]+pars[4]*GAU_fitted), log=TRUE)
504 }
```

---

<sup>4</sup>Note that there is still a variance trend in the standardized residuals—rather unsatisfying! I have been through this backwards and forwards and my take is that this is a product of the sample size imbalance between small and large plants. The quantile regression is doing its best. SPE: I think a lot of it has to do with the fitted SD function. `gam(family="gaulss")` says the standard deviation flattens out near the bottom, and using that SD function there is a smaller (but still unsatisfying) variance trend in the standardized residuals.

505 The mean of the JSU is set to that of the best Gaussian model (GAU\_fitted) and the  
506 standard deviation is a function of the mean according to the coefficients (GAU\_sd\_coef)  
507 estimated through iterative re-weighting. Based on diagnostics of the standardized resid-  
508 uals (Fig. 9), JSU parameters that control skewness and kurtosis are defined as linear  
509 functions of the mean, and those coefficients are estimated by maximum likelihood. This  
510 approach relies on the robustness of Gaussian models fitted mean and variance to devia-  
511 tions from normality. If one is skeptical of this approach, it is possible to simultaneously  
512 re-fit all parameters of the JSU in a maximum likelihood framework. However, incorpo-  
513 rating random effects into a custom likelihood model is non-trivial (we provide guidance  
514 on one way to do this, using the “shrinkage” approach, in Appendix XX). Therefore a  
515 key advantage of the hybrid approach is convenient retention of the fitted random ef-  
516 fects and associated variance components, which get shuttled from the Gaussian model  
517 into the non-Gaussian model without any fuss (it was critical that we used a parameter-  
518 ization of the JSU for which `mu` is the mean and `sigma` is the standard deviation). And,  
519 if this approach does not “work” (i.e., deviations from normality biased the fitted val-  
520 ues of the Gaussian model) one would quickly find out through the simulation step of  
521 the workflow. In this case, the hybrid JSU model performed well, generating simulated  
522 data that aligned with the real data better than the best Gaussian model, particularly in  
523 **standard deviation<sup>5</sup>** and kurtosis (Fig. 10). **The JSU model has exactly the same mean**  
524 **and standard deviation of future size as the Gaussian, but Fig. 9 uses the quantile-based**  
525 **nonparametric mean and standard deviation.** The results show that even though the  
526 JSU was not fitted to match those, it comes closer than the Gaussian model as a result of  
527 accounting for the skew and kurtosis.

528 The improvement of the JSU over the Gaussian growth model, while visually satis-  
529 fying, had virtually no influence on SIPM results. Models using Gaussian or JSU growth  
530 kernels had nearly identical, monotonic decreases in  $\lambda$  with increasing local density, and  
531 nearly identical wave velocities (Fig. 11). This species has very low mortality risk once  
532 established (mean remaining life expectancy of a median-sized shrub is 24,408 years)  
533 and its population growth and wave expansion are limited by very low seedling recruit-  
534 ment ((Drees et al., 2023)). Weak size-dependence in survival likely explains why the  
535 improvement in growth modeling had little influence on SIPM predictions.

---

<sup>5</sup>I am a little mystified as to why the JSU is so much better. It is literally the same SD in both distributions. SPE: it's the same SD but not the same quantile-based nonparametric SD, and the JSU gets the nonparametric SD better. With the curves offset, you can see that in also does better at the NP mean.

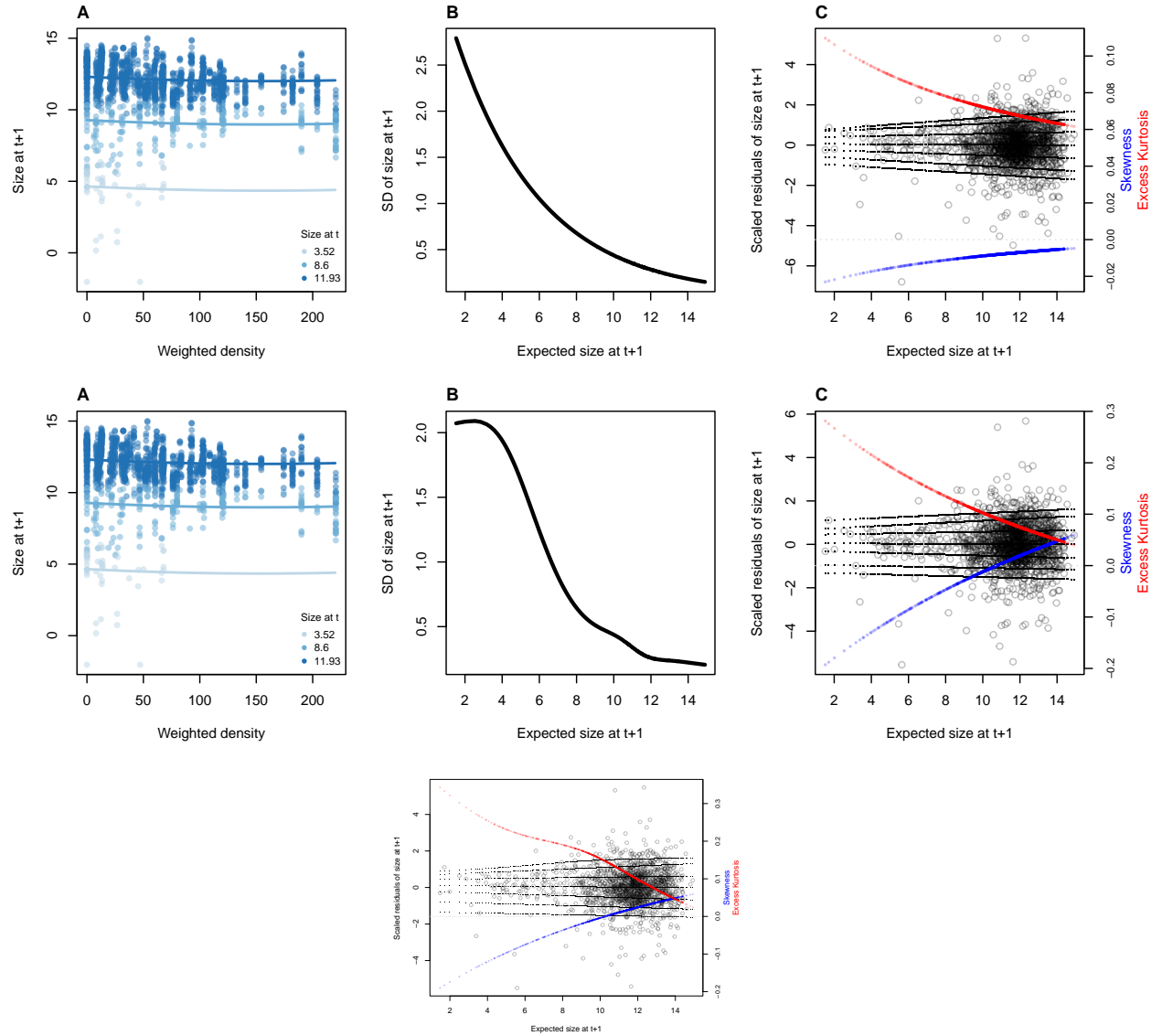


**Figure 9:** Two and 1/3 versions of the same figure. TOP, lmer growth model with log-linear model for SD as a function of fitted. MIDDLE, lmer growth model with spline SD as a function of fitted using gaulss, quantiles from rq (parametric). Bottom: rightmost panel redrawn with spline model for growth and SD using gaulss, and qgam fitting of residual quantiles. **A**, Creosotebush size transition data with respect to initial size (colors) and local weighted density (sum of sizes of all plants within a five-meter transect window). Size is quantified as the natural logarithm of plant volume ( $cm^3$ ). **B**, Standard deviation of size at time  $t + 1$  as a function of expected size at  $t + 1$  (the fitted values), estimated by iterative re-weighting. **C**, Quantile regressions of scaled residuals on size and nonparametric estimates of skewness (blue) and excess kurtosis (red) derived from them. Black lines in **C** show the 5th, 10th, 25th, 50th, 75th, 90th, and 95th quantiles. All figures made by script `creosote_growth_modeling_rq.R`.

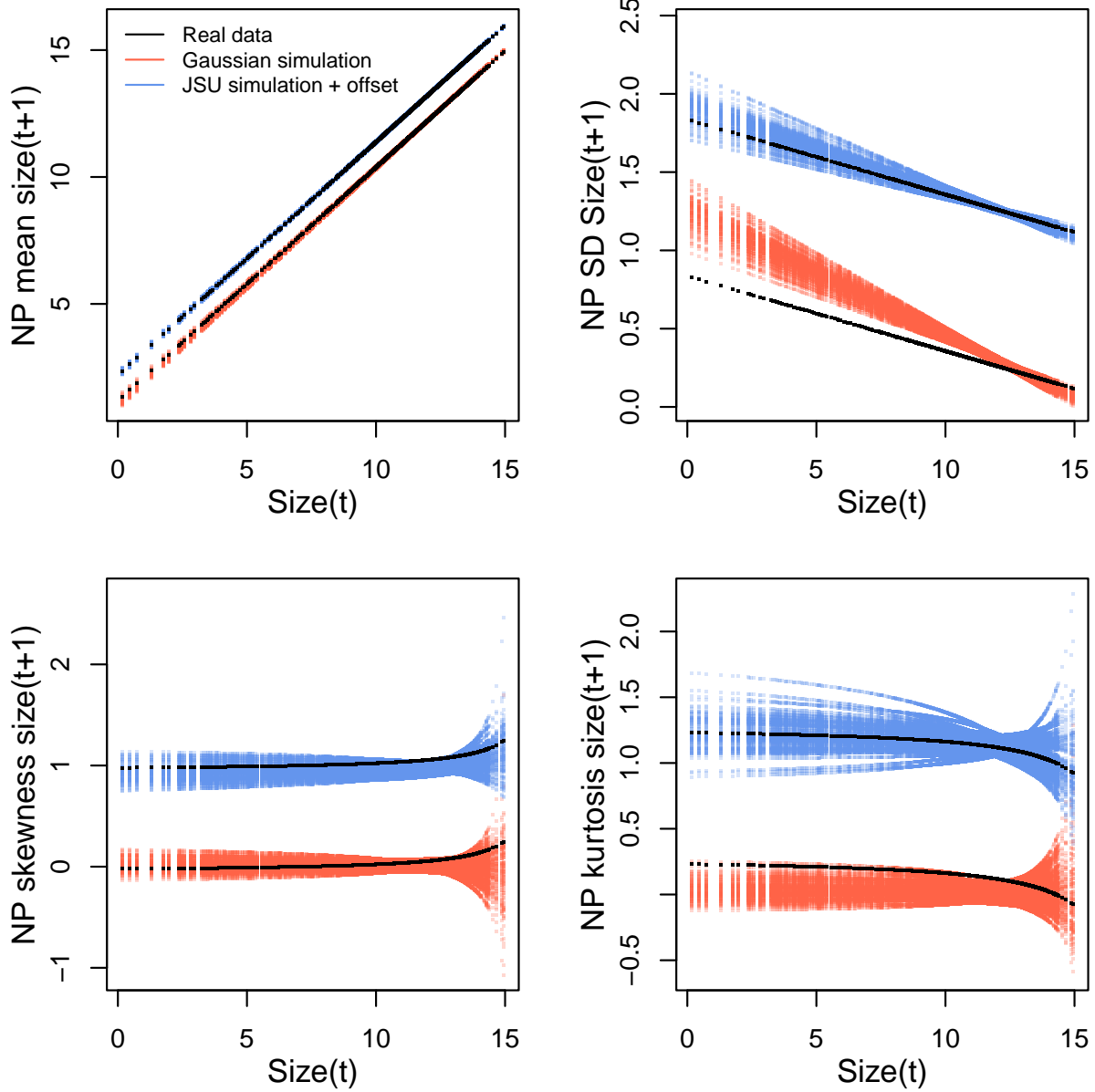


**Figure 10:** Comparisons between real creosotebush data and data simulated from Gaussian and JSU growth models for mean, standard deviation, NP skewness, and NP excess kurtosis of future size conditional on current size. Moments of the future size distribution are plotted with respect to initial size; their distribution is also conditional on density but initial size is by far the stronger predictor of future size, so we chose this visualization. Values for the JSU model (and the corresponding “real data” values) are offset vertically by one unit for comparison. Figure made by script `creosote_growth_modeling_qgam.R`.

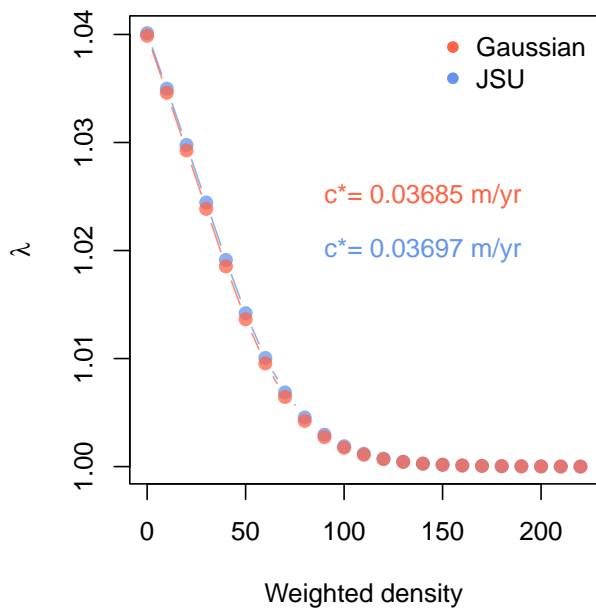


**Figure 11:** Density dependence in fitness ( $\lambda$ ) and asymptotic velocity of the creosote encroachment wave ( $c^*$ ) for Gaussian and JSU growth kernels. Weighted density is the sum of sizes ( $\log(cm^3)$ ) of all conspecifics within a five-meter transect “window”. Figure made by script `creosote_growth_modeling_qgam.R`.

## 536 4 Discussion

537 Much of the appeal of integral projection models has stemmed from their embrace of  
538 continuous size structure through reliance on regression-based approaches, and the po-  
539 tentially complex fixed- and random-effect structures that these approaches allow. Using  
540 familiar statistical tools and with relatively few parameters to estimate, IPM users can  
541 incorporate important sources of variation in demography and interrogate their influ-  
542 ence on ecological and evolutionary dynamics. With this opportunity comes the burden  
543 of getting it right: IPMs are good models of the populations they are intended repre-  
544 sent only insofar as the statistical models provide good fits to the underlying data. The  
545 growth sub-model is the trickiest part of “getting it right” because it defines a distri-  
546 bution of future size conditional on current size. Distributions have many properties –  
547 “moments” – and a good growth model should recapitulate the properties of real size  
548 transitions. The default assumption of normally distributed size transitions, employed  
549 overwhelmingly across 20+ years of IPM studies, is an arbitrary historical precedent.  
550 In four case studies (chosen simply because we had the data at our fingertips) and,  
551 we suspect, more broadly, skewness and excess kurtosis were common features of size  
552 transition data: shrinking was more common than growing, and large changes in size  
553 were more common than a Gaussian model would predict. Our most important mes-  
554 sage is that the standard assumption of normally-distributed size transitions should be  
555 abandoned and a more inquisitive process of growth modeling should take its place.

556 We have attempted to lay out a general workflow for what that process should look  
557 like, guided by visual diagnostics of standardized residuals. One implication of relying  
558 on visual diagnostics is that goodness of fit is in the eye of the beholder. This approach  
559 can empower IPM users to make informed choices, but it is not very prescriptive: we  
560 have not suggested any hard rules for when one or another distribution should be used,  
561 only that a good growth model should generate data that look like the real thing. Al-  
562 ternatively, model selection could be used to identify best-fitting growth distributions  
563 and best-fitting functions for higher moments. However, model selection among growth  
564 distributions with 3-5 parameters, each of which may be functions of state variables or  
565 fitted values, can quickly explode in complexity, and we are not convinced it is worth  
566 the trouble. It is possible to find a good growth model without worrying about which  
567 one is “best”.

568 In all of our case studies, non-Gaussian growth models always yielded more sat-  
569 isfying fits to size transition data than the Gaussian models published in those papers.  
570 However, much to our relief, none of these re-analyses yielded a “gotcha” result that

571 overturned results of the original study. In this small sampling of case studies, im-  
572 proved growth modeling had only modest effects on IPM results. We caution against  
573 taking too much comfort in this outcome; we can imagine other scenarios in which the  
574 choice of the growth distribution could be more consequential. It is worth noting that  
575 three of our case studies focused on perennial plants and the fourth focused on corals,  
576 which are demographically similar to perennial plants (heavy losses during recruitment  
577 but high survival once established). Life cycles such as these may be relatively robust to  
578 subtle features of the growth kernel. More systematic comparative analyses across may  
579 provide insight into which types of species and life histories are more likely to exhibit  
580 strong skewness and kurtosis of size transitions, and the conditions under which demo-  
581 graphic analysis is more or less sensitive to these features of size transition. It is also  
582 worth noting, as we saw in several case studies, that different outputs from the same  
583 model can be more or less sensitive to the choice of growth distribution.

584 Some issues to be discussed.

- 585 • Many software options: lme4/maxLik, mgcv, rstan
- 586 • Comparison of our approach with beta regression method.
- 587 • We have emphasize growth but same principles apply to other continuous state  
588 transitions, eg disease IPMs.
- 589 • Eviction still a problem for unbounded distributions.

## 590 Acknowledgements

591 This research was supported by US NSF grants DEB-1933497 to SPE and DEB-1754468,  
592 2208857, and 2225027 to TEXM.

## 593 5 Authorship statement

594 All authors discussed all aspects of the research and contributed to developing methods,  
595 analyzing data, and writing and revising the paper.

## 596 6 Data accessibility statement

597 No original data appear in this paper. Should the paper be accepted, all computer scripts  
598 supporting the results will be archived in a Zenodo package, with the DOI included at

599 the end of the article. During peer review, our data and code are available at [https://github.com/texmiller/IPM\\_size\\_transitions](https://github.com/texmiller/IPM_size_transitions).  
600

601 **Literature Cited**

- 602 Anscombe, F. J. and Glynn, W. J. (1983). Distribution of the kurtosis statistic  $b_2$  for  
603 normal samples. *Biometrika*, 70(1):227–234.
- 604 Bates, D., Sarkar, D., Bates, M. D., and Matrix, L. (2007). The lme4 package. *R package  
605 version*, 2(1):74.
- 606 Bruno, J. F., Ellner, S. P., Vu, I., Kim, K., and Harvell, C. D. (2011). Impacts of aspergillosis  
607 on sea fan coral demography: modeling a moving target. *Ecological Monographs*,  
608 81(1):123–139.
- 609 Compagnoni, A., Bibian, A. J., Ochocki, B. M., Rogers, H. S., Schultz, E. L., Sneck, M. E.,  
610 Elderd, B. D., Iler, A. M., Inouye, D. W., Jacquemyn, H., et al. (2016). The effect of  
611 demographic correlations on the stochastic population dynamics of perennial plants.  
612 *Ecological Monographs*, 86(4):480–494.
- 613 Conn, P. B., Johnson, D. S., Williams, P. J., Melin, S. R., and Hooten, M. B. (2018). A guide  
614 to bayesian model checking for ecologists. *Ecological Monographs*, 88(4):526–542.
- 615 Cooch, E. G. and White, G. C. (2020, accessed 5/17/2020). *Program MARK - a 'gentle  
616 introduction'*. Available at phidot.org.
- 617 Coulson, T. (2012). Integral projections models, their construction and use in posing  
618 hypotheses in ecology. *Oikos*, 121(9):1337–1350.
- 619 Crone, E. E. (2016). Contrasting effects of spatial heterogeneity and environmental  
620 stochasticity on population dynamics of a perennial wildflower. *Journal of Ecology*,  
621 104(2):281–291.
- 622 Czachura, K. and Miller, T. E. (2020). Demographic back-casting reveals that subtle  
623 dimensions of climate change have strong effects on population viability. *Journal of  
624 Ecology*.
- 625 D'Agostino, R. B. (1970). Transformation to normality of the null distribution of  $g_1$ .  
626 *Biometrika*, pages 679–681.
- 627 Davis, C. (2015). *sgt: Skewed Generalized T Distribution Tree*. R package version 2.0.
- 628 Drees, T., Ochocki, B. M., Collins, S. L., and Miller, T. E. (2023). Demography and  
629 dispersal at a grass-shrub ecotone: a spatial integral projection model for woody plant  
630 encroachment. *Ecological Monographs*, page e1574.

- 631 Easterling, M. R., Ellner, S. P., and Dixon, P. M. (2000). Size-specific sensitivity: applying  
632 a new structured population model. *Ecology*, 81(3):694–708.
- 633 Elderd, B. D. and Miller, T. E. (2016). Quantifying demographic uncertainty: Bayesian  
634 methods for integral projection models. *Ecological Monographs*, 86(1):125–144.
- 635 Ellis, M. M. and Crone, E. E. (2013). The role of transient dynamics in stochastic popula-  
636 tion growth for nine perennial plants. *Ecology*, 94(8):1681–1686.
- 637 Ellner, S. P., Adler, P. B., Childs, D. Z., Hooker, G., Miller, T. E., and Rees, M. (2022).  
638 A critical comparison of integral projection and matrix projection models for demo-  
639 graphic analysis: Comment. *Ecology*, 103(10):e3605.
- 640 Ellner, S. P., Childs, D. Z., and Rees, M. (2016). *Data-driven Modeling of Structured Popula-  
641 tions: A Practical Guide to the Integral Projection Model*. Springer, New York.
- 642 Gould, W. R. and Nichols, J. D. (1998). Estimation of temporal variability of survival in  
643 animal populations. *Ecology*, 79:2531 – 2538.
- 644 Gu, C. (2013). *Smoothing Spline ANOVA Models*. Springer Science+Business Media, New  
645 York, 2 edition.
- 646 Hadfield, J. D. et al. (2010). Mcmc methods for multi-response generalized linear mixed  
647 models: the mcmcglmm r package. *Journal of Statistical Software*, 33(2):1–22.
- 648 Héault, B., Bachelot, B., Poorter, L., Rossi, V., Bongers, F., Chave, J., Paine, C. T., Wagner,  
649 F., and Baraloto, C. (2011). Functional traits shape ontogenetic growth trajectories of  
650 rain forest tree species. *Journal of ecology*, 99(6):1431–1440.
- 651 Jones, M. and Pewsey, A. (2009). Sinh-arcsinh distributions. *Biometrika*, 96:761 – 780.
- 652 Jones, M. C., Rosco, J. F., and Pewsey, A. (2011). Skewness-invariant measures of kurtosis.  
653 *The American Statistician*, 65(2):89 – 95.
- 654 Jones, O. R., Barks, P., Stott, I., James, T. D., Levin, S., Petry, W. K., Capdevila, P., Che-  
655 Castaldo, J., Jackson, J., Römer, G., et al. (2022). Rcompadre and rage—two r pack-  
656 ages to facilitate the use of the compadre and comadre databases and calculation of  
657 life-history traits from matrix population models. *Methods in Ecology and Evolution*,  
658 13(4):770–781.
- 659 Komsta, L. and Novomestky, F. (2015). Moments, cumulants, skewness, kurtosis and  
660 related tests. *R package version*, 14(1).

- 661 Link, W. A. and Nichols, J. D. (1994). On the importance of sampling variance to inves-  
662 tigations of temporal variation in animal population size. *Oikos*, 69(3):539 – 544.
- 663 Louthan, A. M., Keighron, M., Kiekebusch, E., Cayton, H., Terando, A., and Morris, W. F.  
664 (2022). Climate change weakens the impact of disturbance interval on the growth rate  
665 of natural populations of venus flytrap. *Ecological Monographs*, 92(4):e1528.
- 666 McGillivray, H. (1986). Skewness and asymmetry: measures and orderings. *Annals of  
667 Statistics*, 14:994–1011.
- 668 Metcalf, C. J. E., Ellner, S. P., Childs, D. Z., Salguero-Gómez, R., Merow, C., McMahon,  
669 S. M., Jongejans, E., and Rees, M. (2015). Statistical modelling of annual variation for  
670 inference on stochastic population dynamics using Integral Projection Models. *Methods  
671 in Ecology and Evolution*, 6:1007–1017.
- 672 Miller, T. E. (2020). Long-term study of tree cholla demography in the los pinos  
673 mountains, sevilleta national wildlife refuge. [https://doi.org/10.6073/pasta/  
674 dd06df3f950afe4a4642306182237d13](https://doi.org/10.6073/pasta/dd06df3f950afe4a4642306182237d13).
- 675 Miller, T. E., Louda, S. M., Rose, K. A., and Eckberg, J. O. (2009). Impacts of insect  
676 herbivory on cactus population dynamics: experimental demography across an envi-  
677 ronmental gradient. *Ecological Monographs*, 79(1):155–172.
- 678 Miller, T. E., Williams, J. L., Jongejans, E., Brys, R., and Jacquemyn, H. (2012). Evolution-  
679 ary demography of iteroparous plants: incorporating non-lethal costs of reproduction  
680 into integral projection models. *Proceedings of the Royal Society B: Biological Sciences*,  
681 279(1739):2831–2840.
- 682 Ochocki, B. M., Drees, T., and Miller, T. E. (2023). Density-dependent demography of  
683 creosote bush (*larrea tridentata*) along grass-shrub ecotones. <https://doi.org/10.6073/pasta/ca53c16f16dcf9fb11f3ee99ea5445ac>.
- 685 Ohm, J. R. and Miller, T. E. (2014). Balancing anti-herbivore benefits and anti-pollinator  
686 costs of defensive mutualists. *Ecology*, 95(10):2924–2935.
- 687 Ozgul, A., Childs, D. Z., Oli, M. K., Armitage, K. B., Blumstein, D. T., Olson, L. E., Tul-  
688 japurkar, S., and Coulson, T. (2010). Coupled dynamics of body mass and population  
689 growth in response to environmental change. *Nature*, 466(7305):482–485.

- 690 Peterson, M. L., Morris, W., Linares, C., and Doak, D. (2019). Improving structured  
691 population models with more realistic representations of non-normal growth. *Methods*  
692 in Ecology and Evolution, 10(9):1431–1444.
- 693 Plard, F., Schindler, S., Arlettaz, R., and Schaub, M. (2018). Sex-specific heterogeneity  
694 in fixed morphological traits influences individual fitness in a monogamous bird  
695 population. *The American Naturalist*, 191(1):106–119.
- 696 Rees, M., Childs, D. Z., and Ellner, S. P. (2014). Building integral projection models: a  
697 user’s guide. *Journal of Animal Ecology*, 83(3):528–545.
- 698 Rigby, R. A., Stasinopoulos, M. D., Heller, G. Z., and De Bastiani, F. (2019). *Distributions*  
699 for modeling location, scale, and shape: Using GAMLSS in R. CRC press.
- 700 Salguero-Gómez, R. and Casper, B. B. (2010). Keeping plant shrinkage in the demo-  
701 graphic loop. *Journal of Ecology*, 98(2):312–323.
- 702 Schielzeth, H., Dingemanse, N. J., Nakagawa, S., Westneat, D. F., Allegue, H., Teplitsky,  
703 C., Réale, D., Dochtermann, N. A., Garamszegi, L. Z., and Araya-Ajoy, Y. G. (2020).  
704 Robustness of linear mixed-effects models to violations of distributional assumptions.  
705 *Methods in ecology and evolution*, 11(9):1141–1152.
- 706 Schultz, E. L., Eckberg, J. O., Berg, S. S., Louda, S. M., and Miller, T. E. (2017). Native  
707 insect herbivory overwhelms context dependence to limit complex invasion dynamics  
708 of exotic weeds. *Ecology letters*, 20(11):1374–1384.
- 709 Shriner, R. K., Cutler, K., and Doak, D. F. (2012). Comparative demography of an epi-  
710 phytic lichen: support for general life history patterns and solutions to common prob-  
711 lems in demographic parameter estimation. *Oecologia*, 170:137–146.
- 712 Stasinopoulos, D. M., Rigby, R. A., et al. (2007). Generalized additive models for location  
713 scale and shape (gamlss) in r. *Journal of Statistical Software*, 23(7):1–46.
- 714 Stubberud, M. W., Vindenes, Y., Vøllestad, L. A., Winfield, I. J., Stenseth, N. C., and Lan-  
715 gangen, Ø. (2019). Effects of size-and sex-selective harvesting: An integral projection  
716 model approach. *Ecology and Evolution*, 9(22):12556–12570.
- 717 Wan, X., Wang, W., Liu, J., and Tong, T. (2014). Estimating the sample mean and stan-  
718 dard deviation from the sample size, median, range and/or interquartile range. *BMC*  
719 *medical research methodology*, 14:1–13.

- <sup>720</sup> Williams, J. L., Miller, T. E., and Ellner, S. P. (2012). Avoiding unintentional eviction from  
<sup>721</sup> integral projection models. *Ecology*, 93(9):2008–2014.
- <sup>722</sup> Wood, S. (2017). *Generalized Additive Models: An Introduction with R*. Chapman and  
<sup>723</sup> Hall/CRC, 2 edition.
- <sup>724</sup> Zhang, J. L. (2014). Comparative investigation of three bayesian p values. *Computational  
725 Statistics & Data Analysis*, 79:277–291.

# Appendices

## S.1 The Jones-Pewsey distribution

Jones and Pewsey (2009) introduced a simple, tractable generalization of the Normal distribution with two additional parameters determining asymmetry (skewness), and tail weight (kurtosis) which can be either lighter or heavier than the Gaussian. It is defined as a transformation of a  $\text{Normal}(0,1)$  random variable using the hyperbolic sine function ( $\sinh$ ) and its inverse ( $\text{asinh}$ ), as follows. The distribution family's base probability density  $f_{\epsilon,\delta}$  is the probability density of the random variable  $X_{\epsilon,\delta}$  where

$$Z = \sinh(\delta \text{ asinh}(X_{\epsilon,\delta}) - \epsilon) \quad (\text{S.1})$$

and  $Z$  has a  $\text{Normal}(0,1)$  distribution. Equivalently,

$$X_{\epsilon,\delta} = \sinh\left(\frac{1}{\delta} \text{ asinh}(Z) + \frac{\epsilon}{\delta}\right). \quad (\text{S.2})$$

Parameters  $\delta = 1, \epsilon = 0$  give the  $\text{Normal}(0,1)$  distribution. Skewness has the sign of  $\epsilon$ , and  $\delta > 0$  controls tail weight, with heavier than Gaussian tails for  $\delta < 1$  and lighter than Gaussian tails for  $\delta > 1$ . A formula for the density  $f_{\epsilon,\delta}$  is given by Jones and Pewsey (2009, eqn. 2). The general four-parameter family with location parameter  $\mu$  and scale parameter  $\sigma$  is defined as the probability densities of  $\mu + \sigma X_{\epsilon,\delta}$ . We refer to this as the JP distribution family.

As is unfortunately the case for most four-parameter distributions  $\mu$  is not the mean,  $\sigma$  is not the standard deviation,  $\epsilon$  is not the skew and  $\delta$  is not the kurtosis. All else being equal, larger  $\mu$  gives a larger mean, larger  $\sigma$  gives a higher standard deviation, higher  $\epsilon$  gives higher asymmetry, and higher  $\delta$  gives heavier tail weight. But each moment is jointly determined by all four parameters.

The main advantage of the JP distribution is that the attainable combinations of skewness and kurtosis are very broad, compared to other four-parameter families, and come very close to the theoretical limits on kurtosis as a function of skewness (Jones and Pewsey, 2009, Fig. 2). Additionally, being a transformation of the Normal makes it very simple to generate random numbers from the distribution, and to compute probability density, cumulative distribution, and quantile functions. There are also simple analytic formulas for the first four moments (Jones and Pewsey, 2009, p. 764) which we use below to define a centered and scaled version in which  $\mu$  and  $\sigma$  are the mean and standard deviation.

756        The definition (S.2) shows that the distribution depends on  $\epsilon$  only through the ratio  
 757         $\epsilon/\delta$ . We have found that this property can be problematic for estimating distribution  
 758        parameters. Even with good sized ( $n = 250$  or  $500$ ) data sets generated from the distri-  
 759        bution with known parameters, both maximum likelihood and Bayesian estimation were  
 760        unstable for some values of  $\epsilon$  and  $\delta$ , occasionally yielding estimates far from the truth.  
 761        One cause was a ridge in the  $(\epsilon, \delta)$  likelihood surface with a constant of  $\epsilon/\delta$ . Another is  
 762        that when  $\delta$  is large, changes in  $\epsilon$  have little effect.

763        To avoid that problems, we reparameterize the distribution as follows:

$$764 \quad X_{\lambda, \tau} = \sinh(e^{-\tau} \operatorname{asinh}(Z) + \lambda). \quad (\text{S.3})$$

765        Thus, the two parameterizations are related by

$$766 \quad \delta = e^\tau, \epsilon = \delta\lambda = e^\tau\lambda. \quad (\text{S.4})$$

767        The definition of  $\tau$  allows it to take any real value, with negative values giving thinner  
 768        than Gaussian tails and positive values giving fatter than Gaussian tails.  $\lambda$  also can take  
 769        any real value, and the distribution's skew has the same sign as  $\lambda$ . Because the sinh  
 770        function is nonlinear, it is still the case that the skew depends on  $\tau$  as well as  $\lambda$ , but the  
 771        "crosstalk" between the kurtosis and skew parameters is weaker. As a result, we found  
 772        that maximum likelihood estimation of parameter values was generally more reliable if  
 773        the distribution is parameterized in terms of  $\tau$  and  $\lambda$ .

## 774        S.2 Estimating mixed-effects models using shrinkage

775        Ecologists often fit demographic and other statistical models that include random effects  
 776        terms to quantify variation among years, spatial locations, individuals, etc. Random  
 777        effects are a natural choice when interest centers on the magnitude of variation (e.g., how  
 778        much does mortality vary among years?) rather than individual values (e.g., mortality  
 779        in 2013). They also allow each estimate to "borrows strength" from others, so that (for  
 780        example) the estimate from a year with small sample size (and thus large sampling  
 781        variability) is shifted towards the center of the overall distribution.

782        Specialized software is often used to fit such models, such as the **nlme**, **lme4**, **mgcv**  
 783        and **gamm4** libraries in R, but these only allow a small subset of the distribution families  
 784        we want to consider for modeling growth increments (the **gamLss** package allows many  
 785        distribution families, but in our experience, even when random effects are simple in  
 786        structure the fitting algorithms often fail to converge or fail to find the global optimum).

787 One way past this limitation is Bayesian estimation, using STAN with user-written  
788 (or borrowed) code for the chosen growth distribution (see section XX for an example).  
789 In this appendix we describe another option, introduced by Link and Nichols (1994)  
790 and Gould and Nichols (1998): fitting a fixed-effects model by Maximum Likelihood,  
791 followed by shrinkage of coefficient estimates. None of the ideas here are original. The  
792 material overlaps Appendix S1 of Metcalf et al. (2015), but for completeness we make  
793 it self-contained. Appendix D of Cooch and White (2020) (written by K.D. Burnham)  
794 provides more details and examples in the context of capture-recapture analysis.

795 Here we explain shrinkage using a simple model based on our analysis of *Pseu-*  
796 *doroegneria spicata*. That model includes random effects for between-year variation in  
797 the slope and intercept of future size (log area) as a function of initial size. To keep  
798 the example simple, we assume that initial size and year are the only covariates, and  
799 we assume that growth increments follow a skew-Normal distribution with noncon-  
800 stant variance and constant skew parameter. Code for this example is in the script  
801 `SimpleShrinkageExample.R`. The first part of the script generates an artificial data set  
802 by fitting the model to a subset of the growth data (20th century Control plots), and  
803 randomly generating new “size next year” values for each individual in the actual data  
804 set. The second part contains the “data” analysis.

805 As in our *P. spicata* analysis, we assumed that that the skew and kurtosis parameters  
806 were functions of the location parameter; this dominated ( $\Delta AIC \approx 30$ ) the alternate  
807 model with skew and kurtosis depending on initial size. The analogous Gaussian model,  
808 with constant variance, could be fitted as follows using `lmer`:

809 `lmer(new.size ~ init.size + (init.size|year), data=growthData, REML=TRUE);`  
810 where `growthData` is a data frame holding the data with year as an unordered factor.  
811 For our skew-Normal model, we instead use maximum likelihood with all between-year  
812 variation included as fixed effects. The appropriate design matrix is easily constructed  
813 using the `model.matrix` function:

814 `U = model.matrix(~ year + init.size:year - 1, data=growthData)`

815 If there are  $T$  years, the matrix `U` specified in this way has  $2T$  columns corresponding to  
816  $n$  annual intercepts and  $T$  annual slopes.

817 Using this design matrix, we can readily write a log likelihood function for use with  
818 the `maxLik` package, with a log link function for the variance because it is necessarily  
819 positive:

820 `LogLik=function(pars,new.size,U){`

```

821 pars1 = pars[1:ncol(U)]; pars2=pars[-(1:ncol(U))];
822 mu = U%*%pars1;
823 sigma = exp(pars2[1]+pars2[2]*mu);
824 dSN1(new.size, mu=mu, sigma=sigma, nu=pars2[3], log=TRUE)
825 }

```

826 Parameters and their standard errors can then be estimated with `maxLik`, starting  
827 from a random guess:

```

828 start=c(runif(ncol(U)), rep(0,3))
829 out=maxLik(logLik=LogLik,start=start, new.size=simData$new.size,U=U,
830   method="BHHH",control=list(iterlim=5000,printLevel=1),finalHessian=TRUE);
831 coefs = out$estimate; # parameters
832 V = vcov(out); SEs = sqrt(diag(V)); # standard errors

```

833 In real life we would repeat the optimization several times with several different starting  
834 values, to be confident that the optimal parameter values had been found.

835 Focus now on the year-specific intercept parameters  $\hat{a}_t, t = 1, 2, \dots, T$ . We can view  
836 the year-specific estimates  $\hat{a}_t$  as consisting of unobserved true values  $a_t$  plus sampling  
837 error:

$$838 \quad \hat{a}_t = a_t + \varepsilon_t \quad (\text{S.5})$$

839 Because of the sampling errors, the sample variance of the estimates  $\hat{a}_t$  is an upward-  
840 biased estimate of the true across-year variance in the parameter. That is undesirable if  
841 the model will be used to project how temporal variability affects population dynamics.  
842 However, maximum likelihood estimation gives us an approximate variance-covariance  
843 matrix  $\hat{V}$  of the sampling errors,  $V$  in the code above. With that information, we can  
844 estimate the parameters of a random effects model for the intercept parameters, and  
845 thereby improve the year-specific estimates and the estimate of the across-year variance.

846 The model is as follows. We make the standard mixed-models assumptions that the  
847  $a_t$  are drawn independently from some fixed distribution with unknown variance  $\sigma^2$ .  
848 We also assume that the estimates  $\hat{a}_t$  are unbiased, that is

$$849 \quad \mathbb{E}(\varepsilon_t | a_t) = 0. \quad (\text{S.6})$$

850 These are optimistic assumptions, but not excessively optimistic. Some degree of tem-  
851 poral correlation will often be present, and as we explain at the end, it is theoretically  
852 possible to account for it. Maximum likelihood parameter estimates are not unbiased,  
853 but if the assumptions of maximum likelihood are satisfied the bias is asymptotically

854 negligible compared to the standard error (the bias scales as the inverse of sample size,  
 855 the standard error as the square root of the inverse of sample size).

856 Let  $S^2$  denote the sample variance of the estimates  $\hat{a}_t$ . It can then be shown that

$$857 \quad \mathbb{E}(S^2) = \sigma^2 + \frac{1}{T} \sum_{t=1}^T \mathbb{E}Var(\varepsilon_t) - \frac{1}{T(T-1)} \sum_{i=1}^{j-1} \sum_{j=1}^T \mathbb{E}Cov(\varepsilon_i, \varepsilon_j). \quad (\text{S.7})$$

858 This is eqn. (1) in Gould and Nichols (1998) in our notation, without the term that results  
 859 from temporal autocorrelation.

860 The terms besides  $\sigma^2$  on the right-hand are the expected impact of sampling error  
 861 on the across-year variance of the parameter estimates; their presence makes  $S^2$  a biased  
 862 estimated of  $\sigma^2$ . However, all of those terms correspond to entries in the variance-  
 863 covariance matrix  $V$ . We can therefore use our estimated variance-covariance matrix  $\hat{V}$   
 864 to removes the bias due to sampling variability:

$$865 \quad \hat{\sigma}^2 = S^2 - \frac{1}{T} \sum_{t=1}^T \hat{V}_{t,t} + \frac{1}{T(T-1)} \sum_{i=1}^{j-1} \sum_{j=1}^T \hat{V}_{i,j}. \quad (\text{S.8})$$

866  $\hat{\sigma}^2$  estimates the variance of the distribution from which the  $a_t$  are assumed to be drawn.

867 Using that estimate, we can adjust the year-specific estimates to reduce the ex-  
 868 pected impact of sampling error. Depending on your purposes, there are two possible  
 869 adjustments. The first option is the one used in the popular capture-recapture analysis  
 870 software Mark Cooch and White (2020),

$$871 \quad \tilde{a}_t = \bar{a}_t + \sqrt{\frac{\hat{\sigma}^2}{\hat{\sigma}^2 + \hat{V}_{t,t}}} (\hat{a}_t - \bar{a}_t). \quad (\text{S.9})$$

872 The name “shrinkage” comes from the fact that each estimate is adjusted towards the  
 873 overall mean, with larger adjustments of values that have higher estimated sampling  
 874 error variance,  $\hat{V}_{t,t}$ . This shrinkage estimate has the property that the expected sample  
 875 variance of the adjusted estimates  $\tilde{a}_t$  is very close to  $\hat{\sigma}^2$ , so the  $\tilde{a}_t$  approximate the actual  
 876 amount of parameter variation.

877 The second is to replace  $\hat{a}_t$  by the least-squares estimate of  $a_t$  under the additional  
 878 assumption that the  $a_t$  are drawn from a Gaussian distribution; this is given by

$$879 \quad \tilde{a}_t = \bar{a}_t + \frac{\hat{\sigma}^2}{\hat{\sigma}^2 + \hat{V}_{t,t}} (\hat{a}_t - \bar{a}_t). \quad (\text{S.10})$$

880 This option is theoretically preferable if the Gaussian assumption is reasonable, and you  
881 are more interested in year-specific values rather than across-year variance. However,  
882 Metcalf et al. (2015) found that even (S.9), which does less shrinkage, resulted in a small  
883 downward bias in the temporal variance of population growth rates. This argues for  
884 always using the first option, and we do the same here.

885 We differ from MARK, however, in using (S.8) rather than an iterative method  
886 that takes (S.8) as its starting estimate and refines the estimate by using weighted least  
887 squares based on the current estimate. Metcalf et al. (2015) found, in simulation studies,  
888 that the iterative method was either slightly beneficial or wildly inaccurate. We therefore  
889 advise against it.

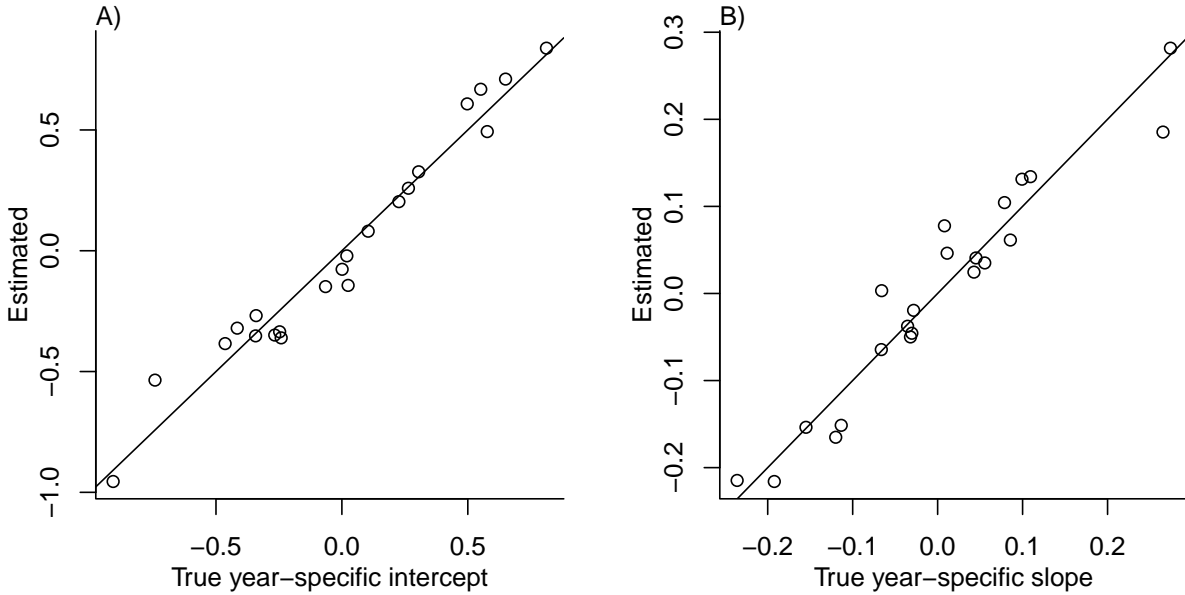
890 Finally, as mentioned above, the estimate of  $\sigma^2$  can account for temporal autocor-  
891 relation in the  $a_t$ . When present, those correlations add a term to eqn. (S.7) (see eqn.  
892 (1) in Gould and Nichols (1998)), which can be estimated from the sample autocorre-  
893 lation of the  $\hat{a}_t$ . We do not recommend doing this (and therefore omit the formulas)  
894 because the autocorrelations can only be reliably estimated if they fall to nearly zero  
895 within lag  $m \ll T$ , in which case the autocorrelation term is small (specifically,  $O(m/T)$ ).  
896 Otherwise, the random error from using poorly estimated autocorrelations is likely to  
897 outweigh the small bias from omitting that term.

898 The take-home message is that estimating random effects from the regression coef-  
899 ficients is very simple:

```
900 # Variance-covariance matrices for intercepts and slopes
901 V1 = V[1:T,1:T]; V2 = V[(T+1):(2*T),(T+1):(2*T)];
902 # Extract year-specific intercepts, center them to zero
903 fixed.fx = coefs[1:T]; fixed.fx = fixed.fx-mean(fixed.fx);
904
905 # Estimate sigma^2
906 var.hat = mean(fixed.fx^2) - mean(diag(V1)) +
907             (sum(V1)-sum(diag(V1)))/(2*T*(T-1));
908
909 # Shrink deviations from the mean
910 shrinkRanIntercept = fixed.fx*sqrt(var.hat/(var.hat + diag(V1)));
911
912 # Do it all again for the slopes
913 fixed.fx2 = coefs[(T+1):(2*T)]; fixed.fx2 = fixed.fx2-mean(fixed.fx2);
914 var2.hat = mean(fixed.fx2^2) - mean(diag(V2)) +
915             (sum(V2)-sum(diag(V2)))/(2*T*(T-1));
```

```
916 shrinkRanSlope = fixed.fx2*sqrt(var2.hat/(var2.hat + diag(V2)));
```

917 The figure below shows the results for one artificial PSSP “data” set, having  $T = 22$   
918 years and growth measurements on about 175 individuals/year on average. The true  
919 random year effects (the ones used to generate the data) are recovered with good accu-  
920 racy and no bias. In particular there is no sign of extreme values being pulled in too  
921 far towards the mean, which would cause an S-shaped graph of estimated versus true  
922 values.



### 923 S.3 Additional case studies

#### 924 S.3.1 Case study: Sea fan corals, *Gorgonia ventalina*

925 Bruno et al. (2011) developed an IPM to understand the rise and fall of a fungal pathogen  
926 *Aspergillus sydowii* in Caribbean sea fan corals *G. ventalina*. The model was based on re-  
927 peated observations of marked corals in permanent transects at several sites near Aku-  
928 mal, Mexico, recording disease status (infected/uninfected) and the area of uninfected  
929 tissue. The epidemic peak had passed and disease incidence was already low, so in-  
930 fected fans were relatively infrequent. We therefore limit the analysis here to uninfected  
931 individuals. Bruno et al. (2011) found statistically significant year and site effects, but  
932 as those explained a very small fraction of the variation in growth increments, they  
933 fitted a single growth model to data pooled across years and sites. We do the same  
934 here. The pooled data set consists of 358 observed size transitions. The data exhibited

935 size-dependent variance in growth (change in area,  $cm^2$ ). Bruno et al. (2011) chose to sta-  
936 bilize the variance by cube-root transforming size, and then fitting the standard model  
937 with Gaussian growth increments. Here we take a different approach, using natural log  
938 transformation of area and modeling size-dependent variance.

939 With initial size as the only predictor, a simple way to fit a Gaussian model with  
940 nonconstant variance is the `gam` function in `mgcv` library (Wood, 2017) using the `gaulss`  
941 family. The mean and standard deviation are both fitted as smoothing spline functions  
942 of initial size, and the `predict` function returns the fitted mean and also the inverse of  
943 the fitted standard deviations with which we can compute the scaled residuals:

```
944 # XH is a data frame holding the data
945 # logarea.t0, .t1 denote initial and final values of log-transformed area
946 fitGAU <- gam(list(logarea.t1~ s(logarea.t0), ~ s(logarea.t0)),
947 data=XH, gamma=1.4, family=gaulss())
948 fitted_all = predict(fitGAU,type="response");
949 fitted_sd = 1/fitted_all[,2];
950 scaledResids = residuals(fitGAU,type='response')/fitted_sd;
```

951 Fig. S-1A shows the log-transformed data and Gaussian model. The mean function  
952 (solid red curve) is visually nearly linear, but the fitted spline is strongly favored over a  
953 linear model for the mean ( $\Delta AIC \approx 9$ ). The spline for standard deviation  $\sigma$  versus initial  
954 size reflects the evident greater variability in growth at smaller sizes.

955 There are no blatant signs of trouble in the pilot Gaussian model, but quantile re-  
956 gressions on the scaled residuals, and the NP Skewness and Kurtosis metrics derived  
957 from them (Eq. 3 and 4), suggest deviations from normality (Fig. S-1B). Specifically,  
958 skewness switches from negative to positive across the size range, with smaller corals  
959 more prone to extreme shrinkage and larger corals more prone to extreme growth. Kur-  
960 tosis also changes direction over the size distribution, with thinner tails than Gaussian  
961 at small sizes and fatter tails at large sizes. The fitted nonparametric moments suggest  
962 that the upper and lower tails of size transition probabilities may differ by up to 20%,  
963 and the weight of the tails may be 20% greater or less than Gaussian, depending on  
964 initial size – not overwhelming deficiencies, but not trivial either. Are these deviations  
965 from normality severe enough to warrant a second, non-Gaussian iteration of growth  
966 modeling? To answer that question, we simulated data from the fitted Gaussian model  
967 and examined whether key properties of the simulated data are consistent with those  
968 of the real data – this is the ultimate litmus test for a growth model's adequacy and  
969 should be a standard element of IPM construction, in our opinion. If the simulated data

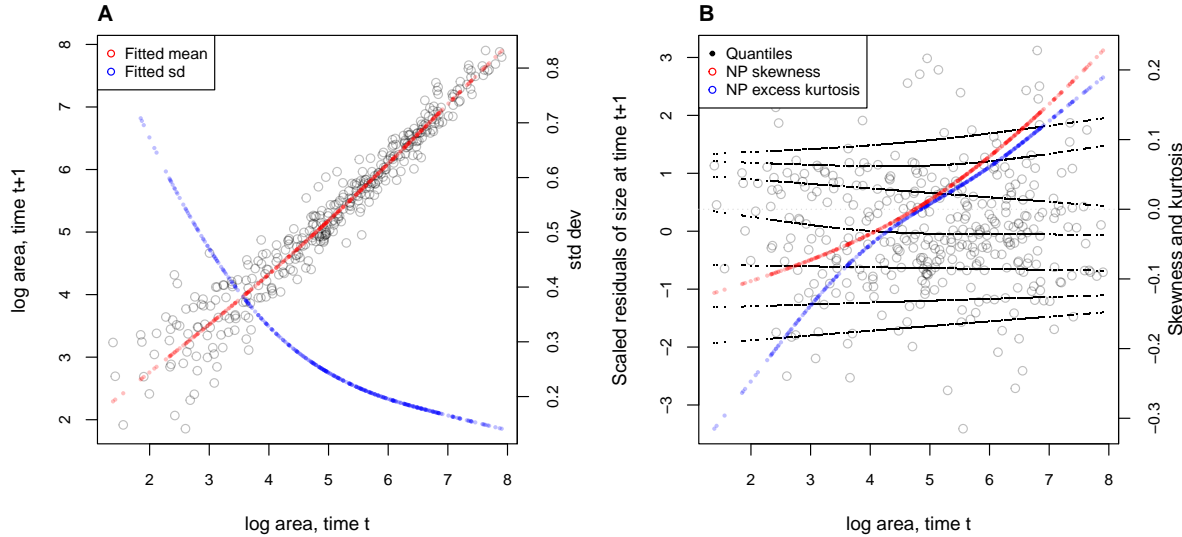


**Figure S-1:** **A**, Size transition data for sea fan corals, *Gorgonia ventalina*, and fitted gam with mean (red) and standard deviation (blue) of future size conditional on current size. **B**, Quantile regressions of scaled residuals on size and nonparametric estimates of skewness (red) and excess kurtosis (blue) derived from them. Black lines in **B** show the 5th, 10th, 25th, 50th, 75th, 90th, and 95th quantiles. Figure made by script AkumalCorals\_qgam.R.

are not consistent with the real data, it is time to choose a better distribution (Fig. 1). In this case, most of 100 Gaussian model simulations are out of line with the skew at smallest and largest sizes, and excess kurtosis observed at moderately large sizes (Fig. S-2 CD). For at least some parts of the size distribution, a non-Gaussian model would better capture size transitions.

We sought a distribution that could accommodate the observed changes in the sign of skewness and excess kurtosis. We chose the sinh-arcsinh (SHASH) distribution, a four-parameter distribution that, conveniently, is included in **mgcv**'s **gam()** function. For consistency with the Gaussian for location and scale, specification of basis functions ( $k = 4$ ) is limited to parameters for skewness and kurtosis:

```
fitSHASH <- gam(list(logarea.t1 ~ s(logarea.t0), # <- location
~ s(logarea.t0), # <- log-scale
~ s(logarea.t0,k=4), # <- skewness
~ s(logarea.t0,k=4)), # <- log-kurtosis
data = XH, gamma = 1.4, family = shash, optimizer = "efs")
```

The fitted model's mean and variance are nearly identical to the Gaussian (Fig. S-2AB), and the fitted trends in skewness and kurtosis are much less "wiggly" than the estimate

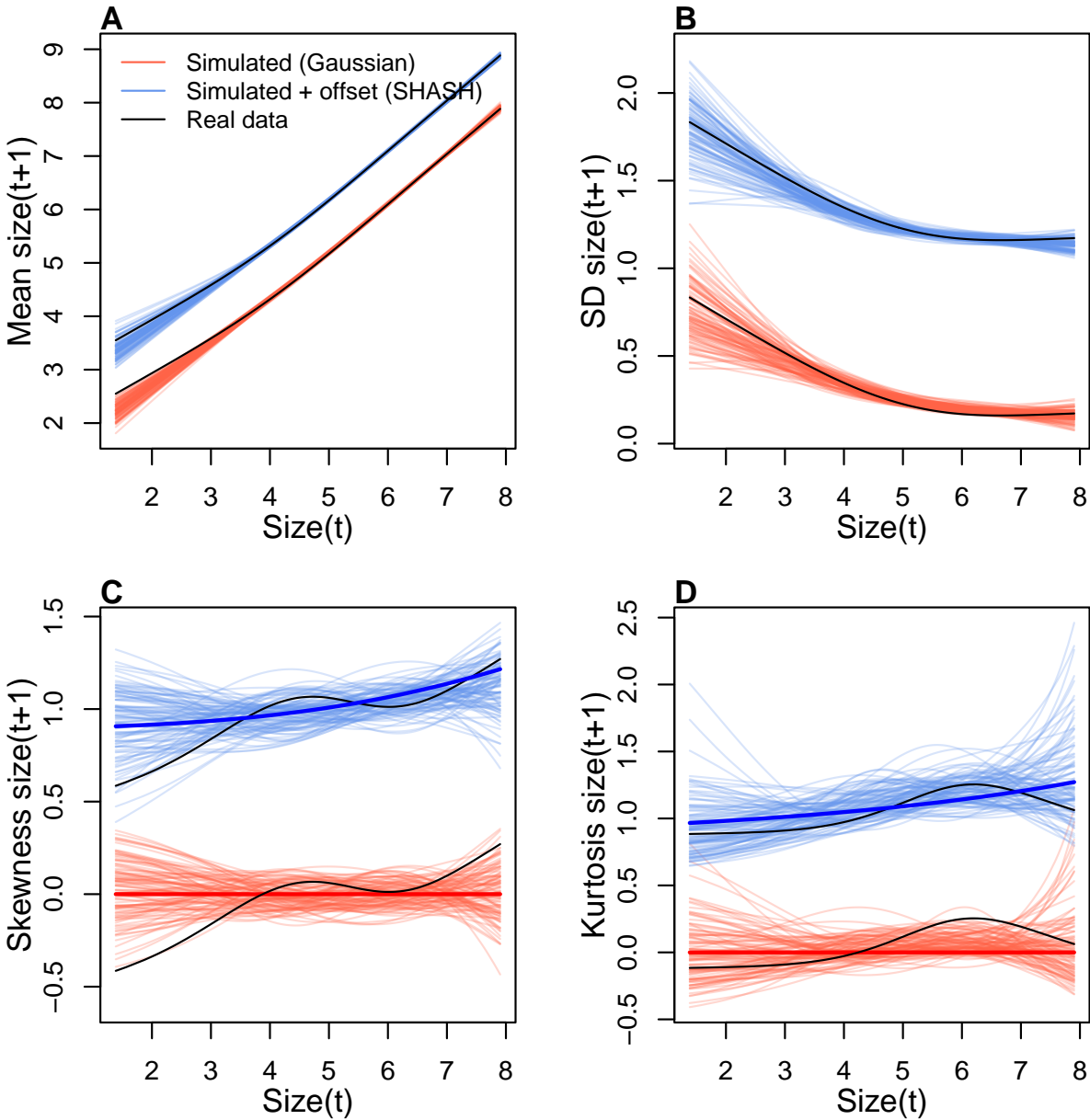


**Figure S-2:** Comparisons among real coral data and data simulated from Gaussian and SHASH growth models for mean, standard deviation, NP skewness, and NP excess kurtosis of future size conditional on current size. Note that plotted values for the SHASH are offset by one unit to allow comparisons. In the skewness and kurtosis panels, the darker solid curves show the values for the fitted growth models. Figure made by script AkumalCorals\_qgam.R.

from the data (Fig. S-2CD). Nonetheless, data simulated from the SHASH model are more consistent with the real data, with more SHASH data sets matching or exceeding the largest skewness and kurtosis values observed (Fig. S-2CD). If one cares to quantify

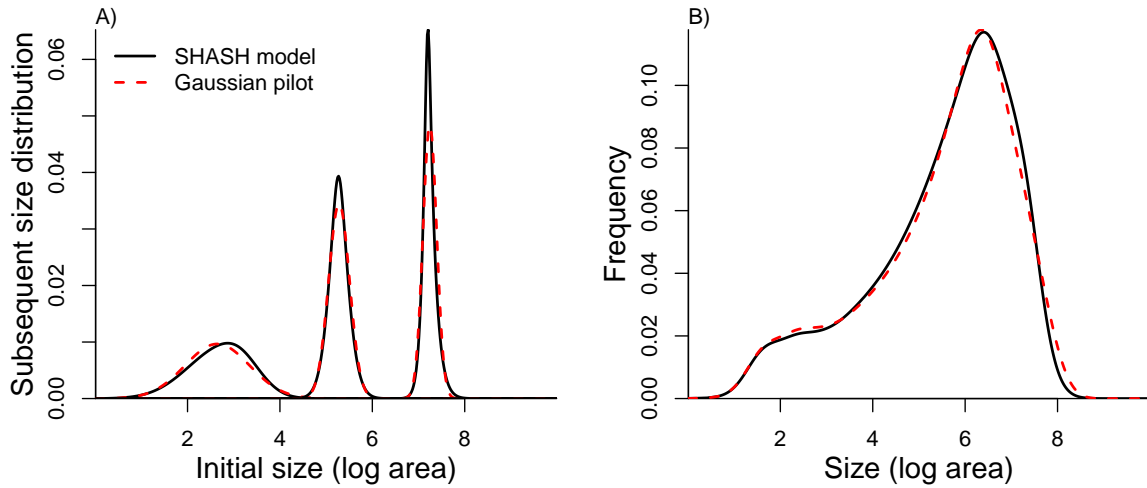


**Figure S-3:** Comparisons between the fitted SHASH growth model (solid black curves) and the Gaussian pilot model (dashed red curves) for sea fans *G. ventalina*. A) Predicted frequency distributions of size in year  $t + 1$  for three different values of size in year  $t$ . The leftmost pair of curves are for initial size equal to the median size of a new recruit (data from (Bruno et al., 2011)); central pair is for the median initial size of uninfected individuals; rightmost pair are for the 95th percentile initial size for uninfected individuals. B) Steady-state size distributions resulting from a constant unit input of new recruits. As in Bruno et al. (2011) we assume that larvae are very widely dispersed, so that the number of recruits arriving at any one location is independent of the local population abundance or structure. Size distribution of recruits was described by a kernel density estimate based on the measured sizes of known new recruits ( $n = 9$ ). Figure made by script AkumalCoralsIPMs.R.

990 the difference between models, the SHASH model is clearly favored by AIC ( $\Delta AIC =$   
 991 5.45) despite having twice as many parameters to fit.

992 What, then, have we gained by fitting a better growth model? Fig. S-3A compares  
 993 the predicted distributions of subsequent size in the fitted model and Gaussian pilot  
 994 models, for the median size of a new recruit (leftmost pair of curves), the median ini-  
 995 tial size (central curves), and the 95th percentile of initial size in the data (rightmost  
 996 curves). The differences are small, and most pronounced for the smallest size, where re-  
 997 cruits are predicted to grow slightly larger under the SHASH model than the Gaussian  
 998 model. The direction of this difference was surprising, because the SHASH has negative  
 999 skew at small sizes in the data. However, the SHASH model also gives a better pre-  
 1000 diction of mean growth at small sizes than the Gaussian model. At intermediate sizes the  
 1001 predictions are nearly identical; at large sizes the SHASH has slightly lower standard  
 1002 deviation, but fatter tails (excess kurtosis). Fig. S-3B shows the predicted steady-state  
 1003 size distributions resulting from a constant unit input of recruits. Again, the differences

1004 are very subtle. Finally, the Gaussian and SHASH growth models predict very similar  
1005 mean life span (17.7 and 17.9 years, respectively).

1006 From these outputs, there is little evidence that improved modeling of coral growth  
1007 meaningfully improved biological inferences from the IPM. One could argue that it was  
1008 not worth the trouble, even though it was almost no trouble at all. But before fitting  
1009 the SHASH model, we could not have known whether or not it would have made a  
1010 difference.

1011 In this case study we used `gam` to fit both the Gaussian and SHASH models because  
1012 that obviated model selection on functions for mean, variance, and higher moments.  
1013 However, `gam` should be used with caution. Nonparametric regression models notori-  
1014 ously “wag their tails” because the ends of the fitted curve can be pulled close to the  
1015 outermost data points. This is especially problematic for growth modeling, because data  
1016 are typically sparse near the bounds of the size distribution. To minimize the risk of  
1017 overfitting we specified the number of “knots” (`k=4`) and used `gamma=1.4` to overweight  
1018 model degrees of freedom as suggested by Gu (2013, sec. 3.2). But it is always impor-  
1019 tant to plot the fitted splines and make sure they do not wag unrealistically. If they do,  
1020 parametric regression may be a better choice.

### 1021 S.3.2 Case study: lady orchid, *Orchis purpurea*

1022 Our final case study examines selection on life history strategies in the lady orchid *Or-  
1023 chis purpurea*. In a prior study, Miller et al. 2012 contrasted the growth trajectories from  
1024 year  $t$  to  $t + 1$  for plants that did or did not flower in year  $t$ , as a way to quantify costs  
1025 of reproduction. The different growth kernels were then used in an IPM to quantify  
1026 evolutionarily stable life history strategies: the optimal flowering size that balances ben-  
1027 efits of flowering at larger sizes against the risk of dying before reaching those sizes.  
1028 The original study assumed a Gaussian distribution of size transitions and allowed for  
1029 non-constant variance with respect to initial size. Here we re-visit that analysis applying  
1030 our growth modeling workflow to derive improved growth kernels for flowering and  
1031 non-flowering orchids.

1032 The data, originated by Dr. Hans Jacquemyn and used here with permission, come  
1033 from 368 plants in a Belgian population that was censused annually from 2003 through  
1034 2011 (for this reanalysis we are using data only from the “light” habitat). Size was mea-  
1035 sured as leaf area ( $cm^3$ ) summed over all leaves, and we analyzed the natural logarithm  
1036 of total leaf area as the size variable of the IPM.

1037 As a pilot Gaussian approach, we fit six candidate models in which the mean was  
 1038 a function of initial size only, additive effects of initial size and flowering status, and  
 1039 interaction between size and flowering, and the standard deviation was a function of  
 1040 size only (models 1-3) or size and flowering status (models 4-6). All models included a  
 1041 random intercept for year. As another variation on software and an alternative to two-  
 1042 step fitting or iterative re-weighting, here we use `nmle::lme()`, which can simultaneously  
 1043 fit linear predictors for mean and variance. For example, model 1 was:

```

1044 orchid_GAU[[1]]<-lme(log_area_t1~ log_area_t,
1045   weights=varExp(form=~ log_area_t),
1046   random=~ 1|begin.year,data=orchid_grow,method="ML")
  
```

1047 Model 3 (size  $\times$  flowering) was strongly favored, consistent with prior results that non-  
 1048 flowering plants have a growth advantage over flowering plants. Growth variance de-  
 1049 clined with initial size for both reproductive classes (Fig. S-4A-B) and skewness and kur-  
 1050 tosis of the standardized residuals indicate strong deviations from normality (Fig. S-4C-  
 1051 D). For most sizes, left skew and excess kurtosis were more severe for non-reproductive  
 1052 plants, with tail imbalance ca. 10% of their total and tail weights 10–20% fatter than  
 1053 Gaussian.

1054 As improvements, we explored the skewed  $t$  and Johnson's SU distributions, both  
 1055 leptokurtic distributions with flexible skewness. We were happier with the skewed  $t$ ,  
 1056 which we fit in a similar way as we fit the JSU to the creosote data, setting the mean  
 1057 and standard deviation to the Gaussian fits and estimating free parameters controlling  
 1058 skewness and kurtosis:

```

1059     ## log_area_t1 and log_area_t are the size obervations
1060     ## flowering indicates reproductive status at time t (0 or 1)
1061     ## GAU_fitted and GAU_sd are mean and standard deviation from lme
1062     ## pars is a vector of free parameters to be estimated
1063 SSTLogLik=function(pars){
1064   dSST(x=log_area_t1,
1065         mu=GAU_fitted,
1066         sigma=GAU_sd,
1067         nu = exp(pars[1] + pars[2]*log_area_t + pars[3]*as.logical(flowering) +
1068             tau = exp(pars[5] + pars[6]*log_area_t + pars[7]*as.logical(flowering) -
1069             log=TRUE)
1070 }
  
```

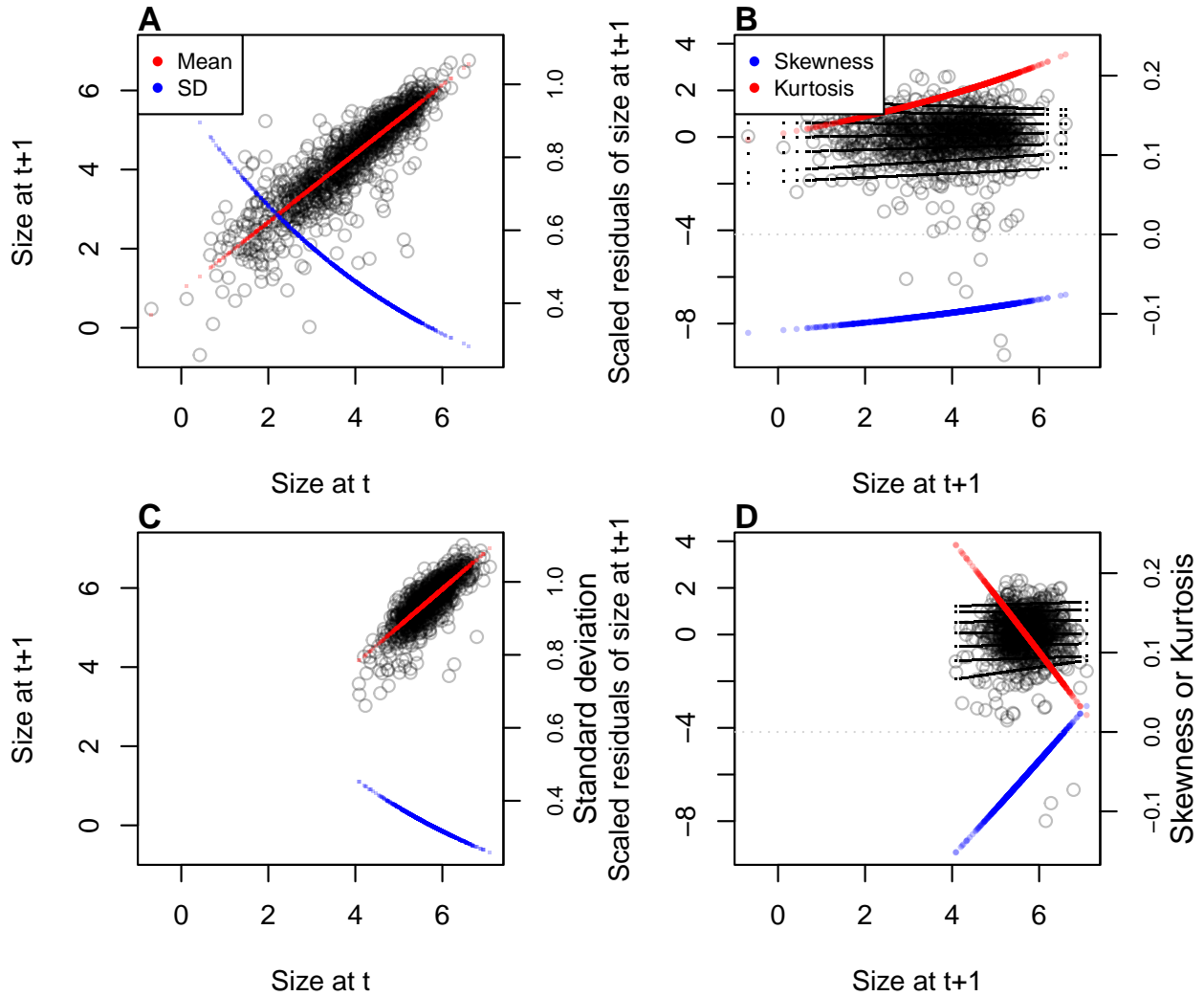
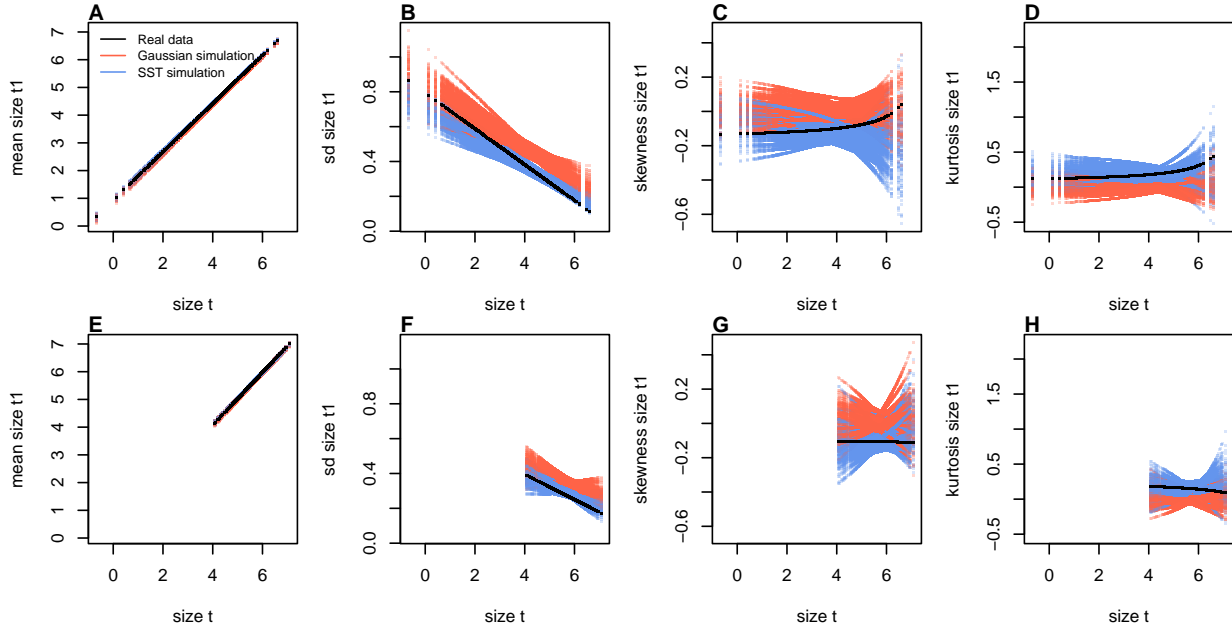


Figure S-4

1071 `gamlss.dist:dSST` is a parameterization of the skewed  $t$  in which `mu` and `sigma` are the  
 1072 mean and standard deviation, respectively. Based on diagnostics of the standardized  
 1073 residuals (Fig. S-4) we allowed `nu` and `tau` to vary by size and differ between flowering  
 1074 and non-flowering plants (note that the `tau` parameter uses a  $\log(x - 2)$  link function).  
 1075 Size transition data simulated from this model corresponded favorably to the real data,  
 1076 much better than the pilot Gaussian model, including improvements in the **standard**  
 1077 **deviation**<sup>6</sup>, skewness, and kurtosis of future size (Fig. S-5).

1078 Finally, we used the improved growth model to revisit key results of the original  
 1079 study. Miller et al. (2012) used the orchid IPM to estimate the evolutionarily stable strat-  
 1080 egy (ESS) as the mean size at flowering that maximizes lifetime reproductive success

<sup>6</sup>Again, the improvement here is surprising to me and I am unsure what to say about it. SPE: again, it's probably about the "usual" mean and SD versus the quantile-based NP versions.



**Figure S-5:** Comparisons between real orchid data and data simulated from Gaussian and skewed  $t$  growth models for mean, standard deviation, NP skewness, and NP kurtosis of future size conditional on current size. Top row (**A-D**) shows plants that were vegetative at the start of the transition year and bottom row (**E-H**) shows plants that were flowering at the start of the transition year. Figure made by script `orchid_growth_modeling_rq.R`.

( $R_0$ ), given the constraint that flowering when small reduces growth and thus elevates mortality risk. Repeating that analysis here, we found that improved growth modeling has virtually no influence on predictions for optimal life history strategies (Fig. S-6). ESS flowering sizes were nearly identical between IPMs with Gaussian vs skewed  $t$  growth models, and both aligned well with the observed mean flowering size (dashed vertical line in Fig. S-6A). Extending beyond the original study, we also explored expected remaining lifespan for different ages and sizes (R package **Rage** (Jones et al., 2022)). Gaussian and skewed  $t$  growth models predicted nearly identical mean remaining lifespans across the stage and size distribution (Fig. S-6B). However, the skewed  $t$  model predicted consistently greater variance in remaining lifespan, nearly 10% greater at some sizes.<sup>7</sup> Thus, as we have seen in other case studies, the practical consequences of improved growth modeling depend on what one aims to learn from the IPM.

<sup>7</sup>*Do not believe this result! I have left it here as a placeholder because I would like to do this correctly. But I think there are problems with Rage's `life_expect_var()` function. The predicted variance declines linearly with matrix dimension.*

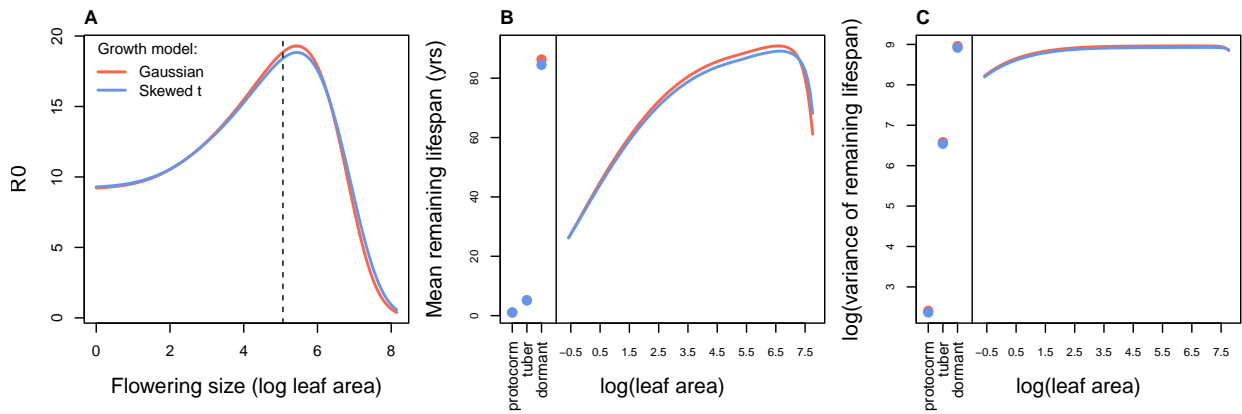


**Figure S-6:** Orchid life history results from IPMs using Gaussian or skewed *t* growth models. **A**, Lifetime reproductive success ( $R_0$ ) as a function of mean size of flowering. Dashed vertical line shows the observed mean flowering size. **B-C**, Mean and variance of remaining lifespan as a function of size or stage. The orchid IPM includes three discrete below-ground stages (protocorm, tuber, and dormant plant) in addition to continuous size of above-ground plants. **SPE: the variance of lifespan results are now correct, using Chrissy Hernandez's functions instead of RAGE. And the result is, non-Gaussian again has no effect.**